UNIVERSITÀ DEGLI STUDI DI PADOVA

FACOLTÀ DI INGEGNERIA

CORSO DI LAUREA IN INGEGNERIA MECCATRONICA

TESI DI LAUREA MAGISTRALE

LOW TEMPERATURE TESTS ON PMMA NOTCHED BARS SUBJECTED TO TORSION

Relatore: Ch.mo Prof. FILIPPO BERTO

Correlatore: Ch.mo Prof. DAVID A. CENDÓN

Correlatore: Ch.mo Prof. MANUEL ELICES CALAFAT

Laureando: GIULIO FIORETTO

Matricola 626218-IMC

ANNO ACCADEMICO 2012-2013

To my granny, Marcella

Low temperature tests on PMMA notched bars subjected to torsion

Giulio Fioretto

Abstract

Fracture behaviour of polymethyl-methacrylate (PMMA) under torsion loading is investigated experimentally and theoretically using axisymmetric specimens weakened by sharp and blunt-tip notches. PMMA specimens were tested at room and low temperature (-60^{o}C). The purpose of the present work is twofold. First, to present a new set of experimental data from PMMA notched samples with different values of notch opening angles, root radii and notch geometries (U, V and semicircular), which should be useful to engineers engaged with static strength analysis of PMMA components. At the best of author knowledge, few data from notch specimens under torsion are available in the literature for this material. Second, to apply to the torsion loading case a fracture criterion based on the strain energy density (SED) averaged over a well-defined control volume surrounding the notch tip, extending what was made in [25, 29, 35] for in-plane tension-shear loading conditions in notched PMMA specimens. Good matching is found between the experimental data related to the critical loads to failure and the theoretical assessments based on the constancy of the mean SED over the material-dependent control volume.

Contents

List of Figures

List of Tables

Chapter 1

Introduction

Since 1960, fracture mechanics theories have been developed to account for various types of non-linear material behaviour (i.e. plasticity, viscoplasticity and viscoelasticity) as well as dynamic effects. All of these more recent results, however, are extensions of Linear Elastic Fracture Mechanics (LEFM).

The development of LEFM during the past century, offered the possibility for a design based on damage tolerance. Such approach is based on the use of the Stress Intensity Factor and the Fracture Toughness as a material property in order to assess the structural integrity of a certain piece [14].

Although this methodology of structural integrity assessment quickly became very popular, in principle it can be only applied to cracks, that is to say, to very sharp flaws (defects) embedded within the material. Experiments by Leonardo da Vinci, Griffith and others indicated that the discrepancy between the actual strengths of brittle materials and theoretical estimates (approximately E/π - E is the Young's Modulus) was due to flaws in these materials (experimental fracture strengths are tipically three or four order of magnitude below). Fracture cannot occour unless the stress at the atomic level exceeds the cohesive strength of the material. Thus the flaws must lower the global strength by magnifying the stress locally [11].

Besides cracks, common engineering practice requires the machining on many pieces of some details such as holes, U-notches, V-notches, etc. that can be considered as defects in the sense that they act as stress concentrators, although they are intentionally included in the piece. As stress concentrators they can lead to a premature and unforeseen catastrophic failure of a structure.

Despite these kind of defects are relatively common, the knowledge achieved by Fracture Mechanics about them is considerably less than the knowledge about theoretical cracks. Under linear elastic conditions (or small scale plasticity around the defect tip), if the defect tip is sharp (zero radius) notch stress intensity factors can be used in the same sense than a Stress Intensity Factor that is used for cracks. As the radius of the defect tip increases, the stress singularity vanishes and the validity of this approach decreases. To overcome this issue many proposals have been made to find the critical load that causes failure on a piece having a U-shape or V-shape notch: the critical value of some

macroscopic stress [2], stress intensity factors [3], strain energy density [4-5] or Cohesive Crack Model [6] among others.

The problem becomes more complex when the piece is subjected to torsion loading. While some data can be found in the literature about U and V notches subjected to Mode I, Mode II and Mixed Mode (I+II) loading, the results about Mode III loading are very limited.

The main purpose of this work is to provide experimental data of blunted notched specimens failure subjected to torsion (Mode III). In order to obtain a wide range of stress concentrations, different notch geometries and notch tip radii have been tested. PMMA has been chosen for such purpose since it can be easily machined. This kind of material is used in a wide range of fields like, for instance, biomechanics [23, 24] or microelectronics [28, 34] fields. At room temperature the stress-strain behaviour of the material on these conditions is far from being linear elastic. In order to get a more brittle and linear elastic material behaviour, besides room temperature, tests were also carried out at -60ºC.

A new set of experimental data from notched samples made of PMMA, with different values of notch opening angles, root radii and notch geometries (U, V and semicircular), will be provided in the experimental results section. The numerical analysis section presents a synthesis of all tests data in terms of averaged SED using a control volume based on the basic material properties under torsion.

Chapter 2

Strain Energy under Mode I loading

The concept of "elementary" volume and "micro structural support length" was introduced by Neuber in 1958 [1]. Neuber formulated the idea that the material is sensitive to a fictitious root radius ρ_f which was given according to the expression $\rho_f = \rho + s\varepsilon$, where ρ is the actual radius, s a factor that takes into account the state of multiaxility and ε the "micro structural support-length". This length depends on the material and not on the notch geometry [7]. The concept of "core region" surrounding the crack tip was proposed in 1973 by Sih [4]. The main idea is that the continuum mechanics stops short at a distance from the crack tip, providing the concept of the radius of the core region. The strain energy density factor S [5] was defined as the product of the strain energy density by a critical distance from the point of singularity. Failure was thought of as controlled by a critical value S_c, whereas the direction of crack propagation was determined by imposing a minimum condition on S.

The strain energy density fracture criterion was refined and extensively summarised in chapter 5 of Sih's book [9]. The material element is always kept at a finite distance from the crack or the notch tip outside the "core region" where the inhomogeneity of the material due to micro-cracks, dislocations and grain boundaries precludes an accurate analytical solution. The theory can account for yielding and fracture and is applicable also to ductile materials.

Different from Sih's criterion, which is a point-related criterion, the averaged strain energy density criterion (SED) as reported in [16, 22] states that brittle failure occurs when the mean value of the strain energy density over a control volume (which becomes an area in two-dimensional cases) is equal to a critical energy W_c. Taking into account a volume of material, and not simply a point at the notch tip, might be the more convenient choice. Over a small but finite volume of material close to the notch, whichever its characteristics (blunt notch, severe notch, corner crack), the energy always has a finite value. In [16] Lazzarin and Zambardi simply suggested using the mean value of the local energy to predict the static and fatigue behaviour of components weakened by sharp V-notches with a strongly variable notch angle. Under mode I conditions, the control radius R_c of the volume, over which the energy was averaged, depends on the ultimate tensile strength and the fracture toughness K_{IC} in the case of static loads and brittle

materials.

The SED approach is based both on a precise definition of the control volume (through the critical radius R_c) and the fact that the critical energy does not depend on the notch geometry and sharpness [29, 33]. Such a method was formalised and applied first to sharp, zero radius, V-notches and later extended to blunt U- and V-notches under Mode I loading [26].

2.1 Analytical Frame

With reference to the coordinate system shown in Fig. 2.1, Mode I stress distribution ahead of a V-notch tip is given by the following expression [17]:

$$\sigma_{ij} = a_1 r^{\lambda_1 - 1} \left[f_{ij}(\theta, \alpha) + \left(\frac{r}{r_0} \right)^{\mu_1 - \lambda_1} g_{ij}(\theta, \alpha) \right] \tag{2.1}$$

where the parameter a_1 can be expressed by the notch stress intensity factor K_I^{V} in the case of a sharp, zero notch radius, V-notch or by the elastic maximum notch stress σ_{max} in the case of blunt V-notches. The eigenfunctions f_{ij} depend only on Williams' eigenvalue λ_1, which controls the sharp solution for zero notch radius. The eigenfunctions g_{ij} mainly depend on eigenvalue μ_1, but are not independent from λ_1. Since $\mu_1 < \lambda_1$, the contribution of μ-based terms in (2.1) rapidly decreases with the increase of the distance from the notch tip[1]. In a generic plane case, the elastic strain energy density $W^{(e)}(r, \theta)$ will depend on Modes I and II and on mixed mode terms. However, only Mode I loading will be considered here. Under the plane strain condition, the eigenfunctions f_{ij} and g_{ij} will satisfy the following expressions[2]:

$$f_{zz}(\theta) = \nu(f_{\theta\theta}(\theta) + f_{rr}(\theta)) \ , \quad g_{zz}(\theta) = \nu(g_{\theta\theta}(\theta) + g_{rr}(\theta)) \tag{2.2}$$

In (2.1) r_0 is the distance evaluated on the notch bisector line between the V-notch tip and origin of the local coordinate system; r_0 depends both on the notch root radius ρ and the opening angle 2α (Fig. 2.1), according to the expression

$$r_0 = \rho \frac{(\pi - 2\alpha)}{(2\pi - 2\alpha)} \tag{2.3}$$

The distance r_0 is maximum when $2\alpha = 0$, $r_0 = \rho/2$, then r_0 progressively decreases [6, 26].

[1] See [16, 17, 26] for a deeper handling.

[2] See Appendix A for the angular functions expressions and for the values of the parameters used in this section

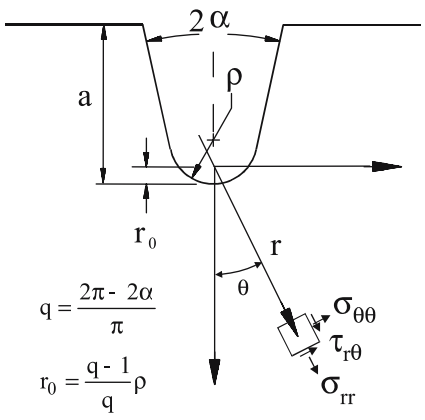

Figure 2.1: Polar coordinates system and stress components.

2.1.1 Sharp V-noches under Mode I loading

The parameter a_1 in (2.1) can be linked to the Mode I notch stress intensity factor (NSIF) by the simple expression

$$a_1 = \frac{K_I^{\mathrm{V}}}{\sqrt{2\pi}} \tag{2.4}$$

where [3]

$$K_I^{\mathrm{V}} = \sqrt{2\pi}\lim_{r\to 0}[\sigma_\theta(r,0)]r^{1-\lambda_1} \tag{2.5}$$

In the presence of a notch root radius equal to zero, the distance r_0 is null, and all μ-related terms in (2.1) disappear. Then the elastic strain energy density under Mode I condition becomes [26]

$$W_1^{(e)}(r,\theta) = \frac{1}{2E}r^{2(\lambda_1-1)}\cdot\frac{(K_I^{\mathrm{V}})^2}{2\pi}[f_{\theta\theta}^2+f_{rr}^2+f_{zz}^2-2\nu(f_{\theta\theta}f_{rr}+f_{\theta\theta}f_{zz}+f_{rr}f_{zz})+2(1+\nu)f_{r\theta}^2] \tag{2.6}$$

The total strain energy over the area of radius R_c is then (Fig. 2.2):

$$E_1^{(e)} = \int_A W_1^{(e)}\,dA = \int_0^{R_c}\int_{-\gamma}^{+\gamma} W_1^{(e)} r\,dr\,d\theta = \frac{1}{E}\cdot\frac{I_1(\gamma)}{4\lambda_1}(K_I^{\mathrm{V}})^2\cdot R_c^{2\lambda_1} \tag{2.7}$$

where the integral I_1 is

$$I_1(\gamma) = \frac{1}{2\pi}\int_{-\gamma}^{+\gamma}[f_{\theta\theta}^2 + f_{rr}^2 + f_{zz}^2 - 2\nu(f_{\theta\theta}f_{rr} + f_{\theta\theta}f_{zz} + f_{rr}f_{zz}) + 2(1+\nu)f_{r\theta}^2]\,d\theta \tag{2.8}$$

In a plane case, the control volume becomes the semicircular sector shown in Fig. 2.2. Its area is

$$A = \int_0^{R_c}\int_{-\gamma}^{+\gamma} r\,dr\,d\theta = R_c^2\gamma \tag{2.9}$$

By using (2.9) the mean value of the elastic strain energy density referred to the area is

$$W_1^{(e)} = \frac{E_1^{(e)}}{A} = \frac{I_1}{4E\lambda_1\gamma}\left(\frac{K_I^{\mathrm{V}}}{R_c^{1-\lambda_1}}\right)^2 \tag{2.10}$$

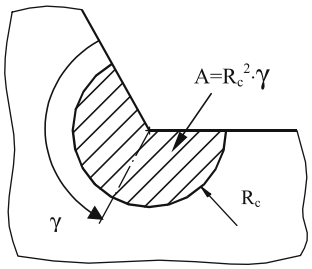

Figure 2.2: Control volume (area) for sharp V-notch.

where λ_1 is Williams' eigenvalue and $\gamma = \pi - \alpha$. Under tensile stresses SED criterion assumes that failure occurs when $\overline{W} = W_c$, where the critical value W_c is a property which varies from material to material. If the material behaviour is ideally brittle, then W_c can be evaluated by using simply the conventional ultimate tensile strength σ_t (measured in direct tensile test on a unnotched, plain specimen), so that:

$$W_c = \frac{\sigma_t^2}{2E} \tag{2.11}$$

Often plain specimens exhibit a non-linear behaviour whilst the behaviour of notched specimens remain linear. Under these circumstances the stress σ_t should be substituted by "the maximum normal stress existing at the edge at the moment preceding the cracking" (see [10]). In [18], Seweryn and Lukaszewicz recommend also to use tensile specimens with semicircular notches. Equation (2.10) makes it possible to determine the critical value of the radius if one knows the experimental values W_c and K_{IC}^{V} that provoke the failure under tensile stresses. If the critical value of the NSIF is determined by means of specimens with $2\alpha \neq 0$, the control radius can be estimated by the expression [16]

$$R_c = \left[\frac{I_1 (K_{IC}^{\mathrm{V}})^2}{4\lambda_1 \gamma E W_c}\right]^{1/[2(1-\lambda_1)]} \tag{2.12}$$

In [26], Lazzarin and Berto give several values of I_1 of (2.12) for sharp V-notches, as a function of the notch angle. We report here only two I_1 usefull values as function of notch angle and poisson ratio:

$$I_1(2\alpha = 0;\ \gamma = \pi;\ \nu = 0.3) = 0.845$$

$$I_1(2\alpha = 135^{\mathrm{o}};\ \gamma = \tfrac{5}{8}\pi;\ \nu = 0.3) = 0.620$$

When $2\alpha = 0$, K_{IC}^{V} equals the fracture toughness K_{IC} [26] (case of plane strain condition). The material control radius can be derived by (2.12) or by using the more elegant expression obtained by Yosibash et al. [22]:

$$R_c = \frac{(1+\nu)(5-8\nu)}{4\pi}\left(\frac{K_{IC}}{\sigma_t}\right)^2 \tag{2.13}$$

An expression analogous to (2.12) has already been used by Lazzarin et al. [16, 19] and Livieri and Lazzarin [27] to analyse fatigue strength data from welded joints made of steel. The welded toe region was modelled as a sharp V-notch with $2\alpha = 135^{o}$. In those cases K_{IC} had been substituted by the critical value of the generalised stress intensity factor range and W_c had been determined on the basis of the fatigue strength range of butt ground welded joints. Both parameters referred to 5 million cycles and a nominal load ratio equal to zero. R_c was found out to be about equal to 0.3 mm for welded joints made of structural steels and about 0.1 mm for welded joints made of some aluminium alloys.

In the present section the strain energy density criterion is thought of to be applied under Mode I stress distribution due to tension or bending loads, Eqs. (2.10)–(2.13), and not to a generic stress state. The cases of pure compression or combined compression and shear, for example, would require a reformulation for R_c and should also take into account the variability of the critical strain energy density W_c with respect to the case of uniaxial tension loads [26]. With reference only to combined tension and shear, Lazzarin and Zambardi discussed and validated the hypothesis of constancy of R_c in [16], by using experimental data mainly due to Seweryn et al. [12]. Seweryn investigated mixed-mode fracture of PMMA specimens with a double symmetric sharp V-notch with an opening angle 2α ranging from 20^{o} to 80^{o}. By modifying the orientation ψ of the specimen axis with respect to the applied tensile force, specimens were loaded in combined tension and shear. At two limit conditions, the middle cross section of the specimens was loaded by pure tension (when $\psi = 0^{o}$) and by pure shear ($\psi = 90^{o}$). All experimental data due to Seweryn were plotted in terms of $\Delta\overline{W} = \Delta\overline{W}_1 + \Delta\overline{W}_2$, showing a weak or absent variability as a function of ψ [16]. Afterwards, the finite volume energy approach was applied to some series of steel welded joints subjected to pure bending, pure torsion and combined in-phase bending and torsion. Once modelled the control volume with a radius R_c about equal to 0.3 mm, the fatigue strength data were found to belong to a single scatter band of limited width [20]. At parity of $\Delta\overline{W} = \Delta\overline{W}_1 + \Delta\overline{W}_3$ and R_c, that did not hold true for combined out-of-phase bending and torsion data. That means that R_c cannot be considered, strictly speaking, independent on the applied load [26]. The same consideration is valid for Neuber's microstructural support length.

2.1.2 Blunt V-noches under Mode I loading

In the presence of rounded V-notches it is possible to link the parameter a_1 of (2.4) to the maximum principal stress present at the notch tip [26]:

$$a_1 = \frac{\sigma_{max} r_0^{1-\lambda_1}}{1 + \tilde{\omega}_1} \tag{2.14}$$

where values of $\tilde{\omega}_1$ are reported in [26]'s *Table 1.*

The elastic strain energy density is given by the following expression:

$$W_1^{(e)}(r,\theta) = \frac{1}{2E}\left(\frac{\sigma_m a x}{1+\tilde{\omega}_1}\right)^2 \left[\left(\frac{r}{r_0}\right)^{2(\lambda_1-1)} \tilde{F}_\lambda + \left(\frac{r}{r_0}\right)^{2(\mu_1-1)} \tilde{G}_\mu + \left(\frac{r}{r_0}\right)^{\lambda_1+\mu_1-2)} \tilde{M}_{\lambda\mu}\right] \tag{2.15}$$

where, following Beltrami's total strain energy criterion, the following relations are valid:

$$\tilde{F}_\lambda = f_{\theta\theta}^2 + f_{rr}^2 + f_{zz}^2 - 2\nu(f_{\theta\theta}f_{rr} + f_{\theta\theta}f_{zz} + f_{rr}f_{zz}) + 2(1+\nu)f_{r\theta}^2$$

$$\tilde{G}_\mu = g_{\theta\theta}^2 + g_{rr}^2 + g_{zz}^2 - 2\nu(g_{\theta\theta}g_{rr} + g_{\theta\theta}g_{zz} + g_{rr}g_{zz}) + 2(1+\nu)g_{r\theta}^2 \tag{2.16}$$

$$\tilde{M}_{\lambda\mu} = f_{\theta\theta}g_{\theta\theta} + f_{rr}g_{rr} + f_{zz}g_{zz} + \\ - \nu(f_{\theta\theta}g_{rr} + g_{\theta\theta}f_{rr} + f_{\theta\theta}g_{zz} + g_{\theta\theta}f_{zz} + f_{rr}g_{zz} + g_{rr}f_{zz})2(1+\nu)f_{r\theta}g_{r\theta}$$

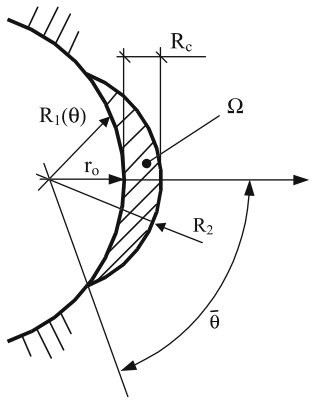

Figure 2.3: Control area for blunt V-notch; material-dependent distance R_c, which is independent of opening angle; radius R_2 intersects the curvilinear notch root edge or the rectilinear part of the V-notch edge.

Considering the area Ω shown in Fig. 2.3 (reminiscent of some very interesting micrographs reported by Gearing and Anand in [21], who dealt with notchsensitive fracture of polycarbonate), the strain energy can be expressed as

$$E_1^{(e)} = \int_\Omega W_1^{(e)}\, d\omega = \int_{-\bar{\theta}}^{+\bar{\theta}} \int_{R_1(\theta)}^{R_2} W_1^{(e)} r\, dr\, d\theta \tag{2.17}$$

In a more explicit form [26]

$$E_1^{(e)} = \frac{1}{2E}\left[\frac{\sigma_{max}\sqrt{2\pi}}{1+\tilde{\omega}_1}\right]^2 r_0^{2(1-\lambda_1)}(I_\lambda + I_\mu + I_{\lambda\mu}) \tag{2.18}$$

where the integrals I_λ, I_μ, $I_{\lambda\mu}$ are defined in [26]. In general it is possible to write:

$$I_1 = \frac{1}{2\pi}(I_\lambda + I_\mu + I_{\lambda\mu}) \tag{2.19}$$

where the introduction of 2π makes I_1 consistent with the expression of the sharp notch case, (2.8). In a synthetic form, the energy in the structural volume can be expressed as

$$E_1^{(e)} = \frac{1}{2E}\left[\frac{\sigma_{max}\sqrt{2\pi}}{r_0^{(\lambda_1-1)}(1+\tilde{\omega_1}}\right]^2 \cdot I_1 \tag{2.20}$$

where I_1, depends on 2α, ρ and R_c. In the case of a U-shaped notch ($2\alpha = 0$), Eq. 2.20 becomes:

$$E_1^{(e)} = \frac{1}{2E}\left[\frac{\sigma_{max}\sqrt{\pi\rho}}{2}\right]^2 \cdot I_1 \tag{2.21}$$

The mean value of strain energy density is then given by:

$$\overline{W}_1^{(e)} = \frac{1}{E}\left(\frac{I_1}{2\Omega}\right)\sigma_{max}^2 r_0^{2(1-\lambda)}\left[\frac{\sqrt{2\pi}}{1+\tilde{\omega}_1}\right]^2 \tag{2.22}$$

The area Ω is defined as follows [26]:

$$\Omega = \int_{R_1(theta)}^{R_2}\int_{-\bar{\theta}}^{+\bar{\theta}} r\, dr\, d\theta. \tag{2.23}$$

Chapter 3

SED extension under Mode III loading

Modelling the material according to a linear elastic law or, alternatively, a Ramberg–Osgood law, the constancy of SED was documented for sharp V-notches under plane strain conditions (large constraint effects). Under torsion loads, however, small scale yielding conditions are difficult to maintain, both under static and medium cycle fatigue loads, and then SED depends on the material law [43].

As shown in Ch. 2 under mode I load conditions, in the SED approach the determination of the control volume is based on the mean values of some material properties (which are typically fracture toughness and the ultimate tensile stress of the plain specimens, as shown by (2.13)). When only failure data from open V-notches are available, R_c can be determined on the basis of some relationships reported in [30], where K_{Ic} is substituted by the critical value of the notch stress intensity factors (NSIFs) as determined at failure from sharp V-notches.

By using SED approach applied to cracked components, in the case of tearing condition, the critical volume is a circle of radius R_{3c} centred at the tip (Fig. 3.1a). For a sharp V-notch, the critical volume becomes a circular sector of radius R_{3c} centred at the notch tip (Fig. 3.1b).

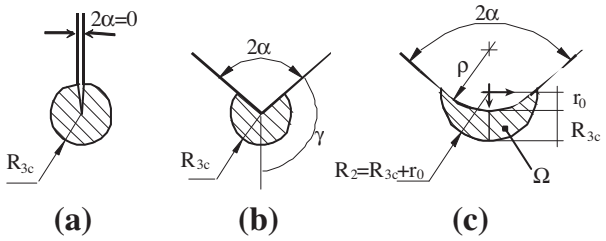

Figure 3.1: Control volume for crack (a), sharp V-notch (b) and blunt V-notch (c) under mode III loading. Distance $r0 = \rho(\pi - 2\alpha)/(2\pi - 2\alpha)$. For a U-notch $r0 = \rho/2$.

Dealing here with sharp notches under torsion loading, the control radius R_{3c} can be estimated by means of the following equation [48]

$$R_{3c} = \left(\sqrt{\frac{e_3}{1+\nu}} \frac{K_{3c}}{\tau_t} \right)^{1-\lambda_3} \tag{3.1}$$

In (3.1) K_{3c} is the Mode III critical notch stress intensity factor and τ_t is the ultimate

shear strength of the unnotched material subjected to torsion. The parameter e_3 quantifies the influence of all stresses and strains over the control volume and $(1-\lambda_3)$ is the degree of singularity of the linear elastic stress fields [13, 33]. Both e_3 and λ_3 depend of the notch opening angle. The values of e_3 and λ_3 are reported in Tab. 3.1 for different opening angles. The mean value of the elastic deformation energy under torsion is[31, 33]:

$$\overline{W}_3 = \frac{e_3}{2(1+\nu)G} \cdot \frac{K_3^2}{R_{3c}^{1-\lambda_3}} \tag{3.2}$$

where K_3 is the mode III notch stress intensity factor and G is the transverse shear modulus. For a blunt V-notch under mode III loading, the volume assumes the crescent shape shown in Fig. 3.1c, where R_{3c} is the depth measured along the notch bisector line. The outer radius of the crescent shape is equal to $R_{3c}+r_0$, being r_0 the distance between the notch tip and the origin of the local coordinate system. Such a distance depends on the V-notch opening angle 2a, according to the expression (2.3), introduced in Ch. 2, page 14.

Table 3.1: Values of the parameters λ_3 and e_3 as a function of the notch opening angles [31].

2α (rad)	λ_3	e_3
0	0.5000	.4138
$\pi/6$	0.5455	0.3793
$\pi/3$	0.6000	0.3448
$\pi/2$	0.6667	0.3103
$2\pi/3$	0.7500	0.2759
$3\pi/4$	0.8000	0.2586

The averaged strain energy density criterion (SED) states that failure occurs when the mean value of the strain energy density over a control volume, $\overline{W}_3$ (see (3.2)), is equal to a critical value W_{3c}, which depends on the material but not on the notch geometry [36]. Under torsion loads, this critical value can be determined from the ultimate shear stress st according to Beltrami's expression for the unnotched material:

$$W_{3c} = \frac{\tau_t^2}{2G} \tag{3.3}$$

3.1 An application case: graphite under torsion loading

With the aim of proving SED criterion for mode III loading, in this section we are showing the results obtained by Berto et al. in [36] by testing round bars of isostatic graphite under torsion loading.

3.1.1 State of the art

Isostatic graphite is manufactured by using cold isostatic pressing technique and is often known for its homogeneous structure and excellent isotropic electrical, thermal and mechanical properties; it is also extensively used in various industrial applications. Graphite has been considered a brittle material in a large body of research. However it best fits a class of materials called *quasi-brittle*. Limited plasticity in the form of microcracking is a sign of such material.

Although cracks are viewed as unpleasant entities (sharp defects ebbedded within the material) in most engineering materials, U- and V-notches of different acuities are sometimes deliberately introduced in design and manufacturing of products made from graphite. A review of literature shows that in spite of extensive studies on mode I and mixed fracture in cracked graphite specimens, there are very few papers e.g [2, 8] focused on brittle fracture of notched graphite components and the notch sensitivity problem.

3.1.2 Graphite test specimens

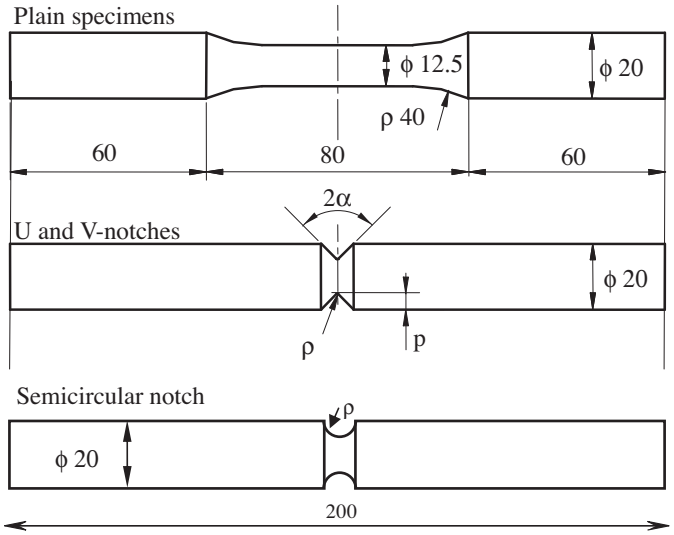

Figure 3.2: Geometry of specimens used in [36].

As shown in Fig. 3.2, different round bar specimens were used for torsion tests: plain specimens, cylindrical specimens with U- and V-notches, and cylindrical specimens with circumferential semicircular notches.

Fig. 3.3 shows some samples of the graphite specimes used in the torsion tests.

3.1.3 SED approach in fracture analysis of the graphite specimens

The SED criterion is employed here to estimate the fracture loads obtained from the experiments conducted by Berto et al. in [36] on the graphite specimens. In order to

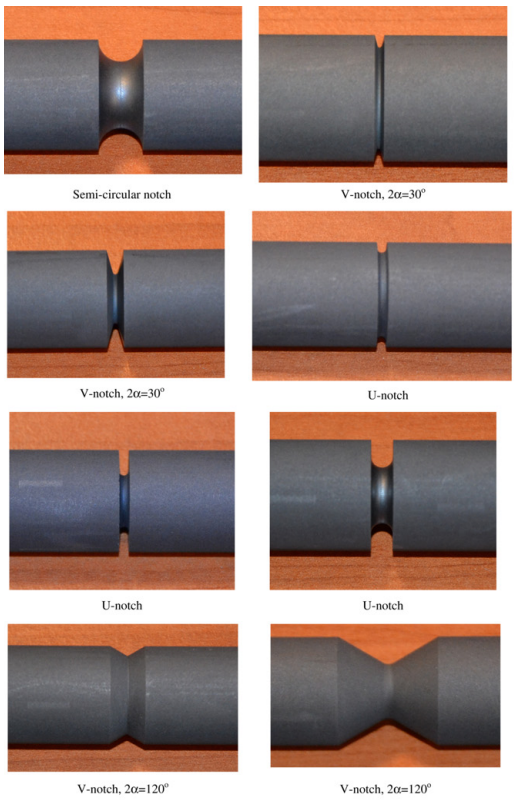

Figure 3.3: Notched specimens used in [36].

determine the SED values, first a finite element model of each graphite specimen was generated. SED criterion states that failure occurs when the mean value of the strain energy density over a control volume, $\overline{W}_3$ (see (3.2)), is equal to a critical value W_{3c} (see (3.3)).

Using the values of $\tau_t = 30$ MPa and $G = 3354$ MPa, the critical SED for the graphite is $W_{3c} = 0.134$ MJ/m^3 [36]. By using (3.1), with $e_3 = 0.379$, $\nu = 0.2$ and $(1 - \lambda_3) = 0.4545$, the radius of the control volume is $R_{3c} = 1$ mm.

Under linear elastic hypothesis, the theoretical load to failure can be easily obtained by a simple proportion between the applied load M in the FE model and square root values of averaged SED, i.e. $M_{th}/M = \sqrt{W_{3c}/\overline{W}}$. These values are given in [36] together with the mean values of the critical loads to failure, $\langle \mathrm{M} \rangle$, of all tested graphite specimens. The values of the SED for the same loads are also given in [36]. It is possible now to compare the SED values at failure with the theoretical value, W_{3c}, as determined by Eq. (3.3).

In Fig. 3.4 are compared the experimental results values of the critical loads (open dots) with the theoreticals predictions based on the constancy of SED in the control volume (solid line).

A synthesis in terms of the square root value of the local energy averaged over the control volume of radius R_{3c}, normalised with respect to the critical energy of the material, is shown in Fig. 3.5. The ratio on the vertical axis is proportional to the fracture load. The aim is to investigate the range of accuracy of all SED-based fracture assessments for the tested graphite specimens. From the figure, it is clear that the scatter of the data is very limited and almost independent of the notch opening angle. Note that 68 out of 70 experimental values fall inside a scatterband ranging from 0.85 to 1.15. Note also that many of the results (about 75%) are inside a scatter ranging from 0.9 to 1.1, which was typical for the notched graphite specimens tested under in-plane mixed tension-shear loading [29].

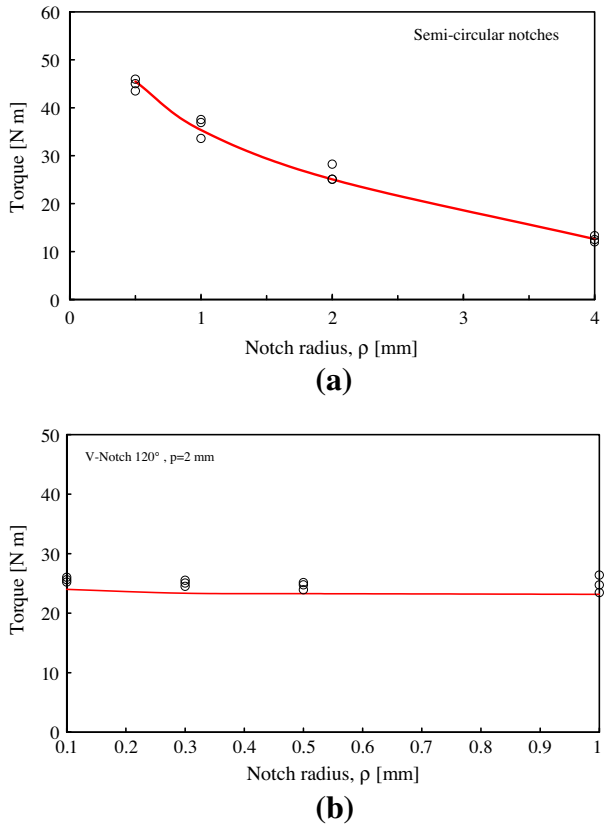

Figure 3.4: Comparsion between experimental data and theoretical assement (solid line) for the graphite specimens used in [36]; semicircualr notches (a), and V-shaped notches with $2\alpha = 120^o$ and notch depth p = 2 mm (b).

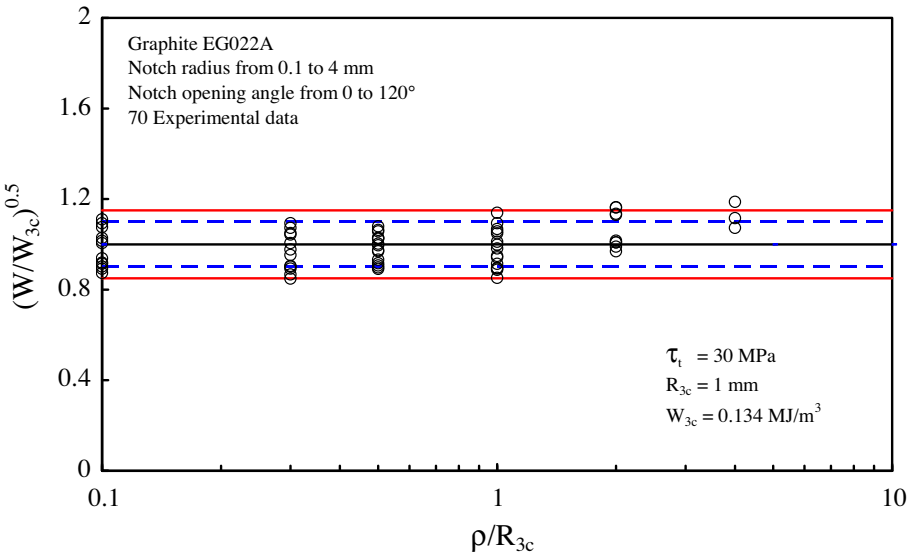

Figure 3.5: Synthesis based on SED of the results from torsion test from [36].

Chapter 4

Experimental Results

In this chapter we are showing the properties and the geometries of the material and how we tested the PMMA specimens in torsion tests.

4.1 Material and Specimens

The material used for the tests was the polymethyl-methacrylate (PMMA), an amorphous glassy polymer. The material tensile properties at room temperature and at -60°C have been obtained in [25] and [35], and are summarized in Tab. 4.1.

Table 4.1: Mechanical properties of PMMA at different temperatures.

Mechanical Properties	**-60°**	**20°**
Elastic Modulus (MPa)	5050	3600
Poisson ratio	0.4	0.4
Tensile strength (MPa)	128.4	74.0
F. toughness (MPa$\sqrt{m}$)	1.7	-

Three different types of specimens were made in order to obtain different stress concentrations: U-notched specimens, V-notched specimens and semicircular notched specimens. The geometry of the specimens is shown in Fig. 4.1.

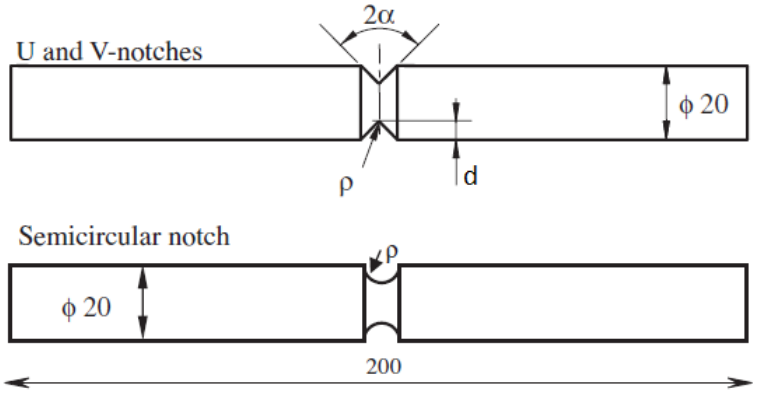

Figure 4.1: Geometry and parameters of the tested specimens.

For the U and V specimens the main parameters defining the notch geometry are the notch depth (d) and the notch tip radius (ρ). In the case of the semicircular notched specimens, the notch tip radius and the depth are identical. Tab. 4.2 summarizes all the combinations of types of notch, notch depths, tip radius and temperatures tested. In order to obtain the material properties needed for the numerical analysis, besides

Table 4.2: Different combinations of geometries and temperatures tested.

Notch type	**d (mm)**	**ρ (mm)**	**20°C**	**-60°C**
Semi-circular	0.5	0.5	Yes	No
Semi-circular	1	1	Yes	No
Semi-circular	2	2	Yes	No
Semi-circular	4	4	Yes	No
Semi-circular	5	5	Yes	Yes
Semi-circular	6	6	Yes	Yes
Semi-circular	7	7	Yes	Yes
U-notch	5	0.3	Yes	Yes
U-notch	5	0.5	Yes	Yes
U-notch	5	1	Yes	Yes
U-notch	5	2	Yes	Yes
U-notch	2	0.3	Yes	Yes
U-notch	2	0.5	Yes	Yes
U-notch	2	1	Yes	Yes
V-notch	5	0.1	Yes	Yes
V-notch	5	0.3	Yes	Yes
V-notch	5	0.5	Yes	Yes
V-notch	5	1	Yes	Yes
V-notch	5	2	Yes	Yes
V-notch	2	0.1	Yes	Yes
V-notch	2	0.3	Yes	Yes
V-notch	2	0.5	Yes	Yes
V-notch	2	1	Yes	Yes

the tests mentioned above, additional torsion tests were carried out on plain cylinders and *quasi-cracked* (narrow V-notch) specimens (Fig. 4.2). The plain cylinder specimens were tested to obtain the maximum torsion strength of all the kinds of PMMA, while cracked specimens were tested in order to obtain the mode III critical stress intensity factor. In Fig. 4.3 are shown the PMMA specimens used in this work. All the specimens were tested at room and low (-60°C) temperature.

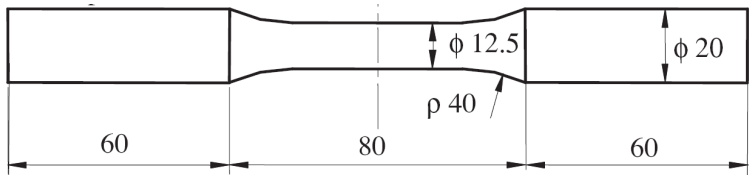

(a) plain specimen

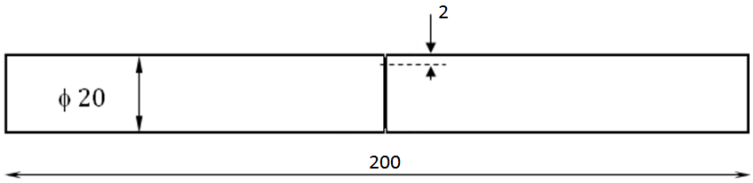

(b) cracked specimen

Figure 4.2: geometry of a) plain cylinder specimens and b) cracked specimens.

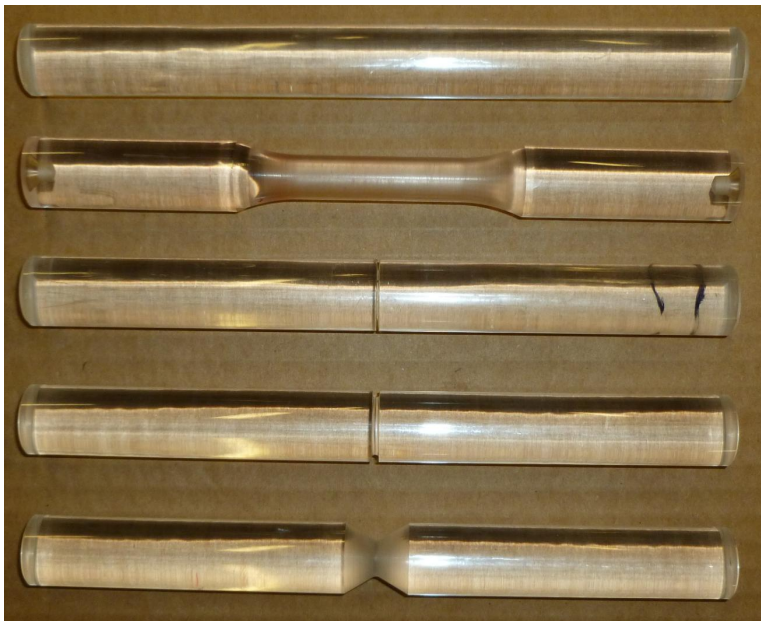

Figure 4.3: PMMA specimens.

4.2 Experimental Setup

4.2.1 Room temperature tests

Room temperature (20ºC) tests were made using a servocontrolled MTS biaxial testing machine. Torque was measured by using a MTS load cell, and the angle on the specimen was registered by a multi-axis extensometer MTS 632.80F-04 with a gauge length equal to 25 mm.

Specimens were put on the machine through hydraulic grips, and then they were tested under angle control, increasing the angle between grips at a constant rate of 2 deg/minute up to failure of the specimen. More details about the experimental procedure can be found in [35].

4.2.2 Low temperature tests

Low temperature tests were made in a mechanical Instron testing machine model TT-D1115 with its own built-in torsion load cell (Fig. 4.4). The angle was measured by a

Figure 4.4: Instron testing machine TT-D1115.

longitudinal Instron 2620-602 extensometer of 12.5 mm gauge length, ±2.5 mm (travel) and 0.15% error at full scale. In order to measure the angle by using this longitudinal extensometer, two especial devices consisting of two identical pieces attached to the specimens at 25 mm distance were devised. Such devices (Fig. 4.5) allowed to translate

the measurement of the extensometer, into the shear angle suffered by the specimen with a gauge length of 25 mm.

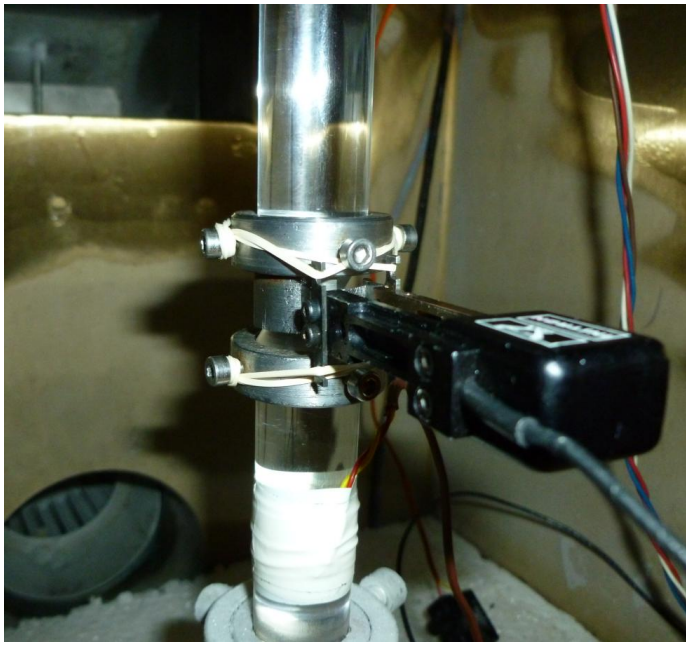

(a)

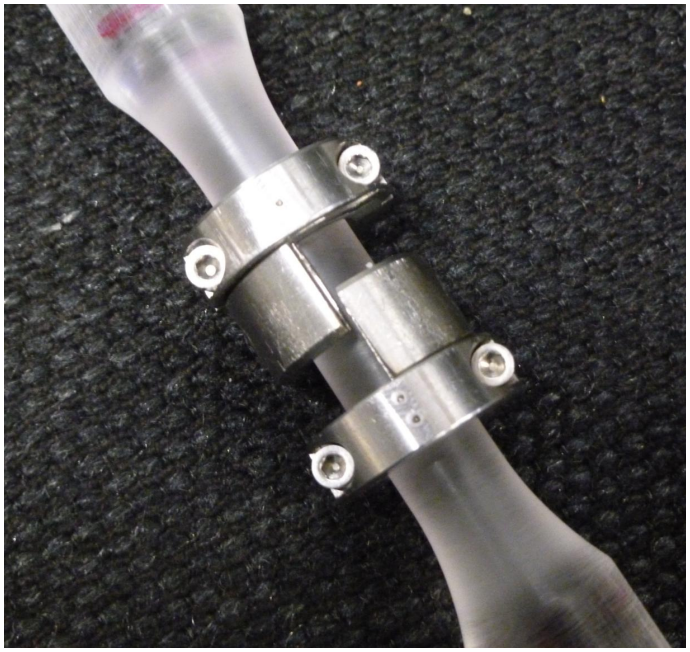

(b)

Figure 4.5: Detail of the devices used to measure the rotation angle in a) 20 mm specimens and b) 12.5 mm unnotched specimens.

Low temperature was reached by controlled injection of liquid N_2 into an Instron environmental chamber (Fig. 4.6).

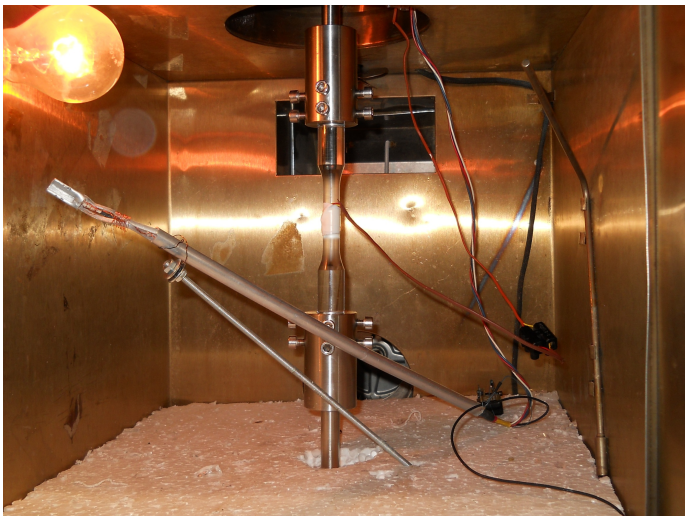

(a) chamber

(b) injection system

Figure 4.6: a) Instron enviromental chamber and b) N_2 injection system.

In order to avoid damage on the specimens due to large thermal stress gradients, temperature was decreased progressively using a constant rate of -1°C/min. Temperature inside the chamber was controlled by using a Pt-100 thermometer. Additionally a thermocouple was attached to the specimen in order to check the temperature on its surface. Once the temperature inside the chamber reached -60°C, it was kept at that constant value. To ensure a regular temperature distribution inside the specimen, this -60°C temperature was kept during 20 minutes from the moment the thermocouple attached to the specimen reached the value of -60°C before starting each test.

Loading was applied by increasing the angle between the grips at a constant rate of 1.8 deg/minute until the specimen was broken.

4.3 Room Temperature Tests Results

Torque versus angle curves obtained at room temperature are plotted in Fig. 4.7, 4.8. For the sake of simplicity, only the results related to 5 mm depth noches and semicircular notches are shown. It is possible finding a more complete coverage of room temperature tests in [35]. Due to the relatively low experimental scatter, only one single curve for each notch geometry is shown. It can be observed how the behaviour is remarkably non linear. Actually, in the case of V and U notched specimens, the maximum load only depends on the notch shape but not on the notch tip radius. This behaviour suggests that a large amount of plasticity/non-linearity is developing on the notched section and all points in this region have a similar stress value, which is governed by the almost constant stress value of the plateau on the material stress-strain curve once plasticity has been fully developed.

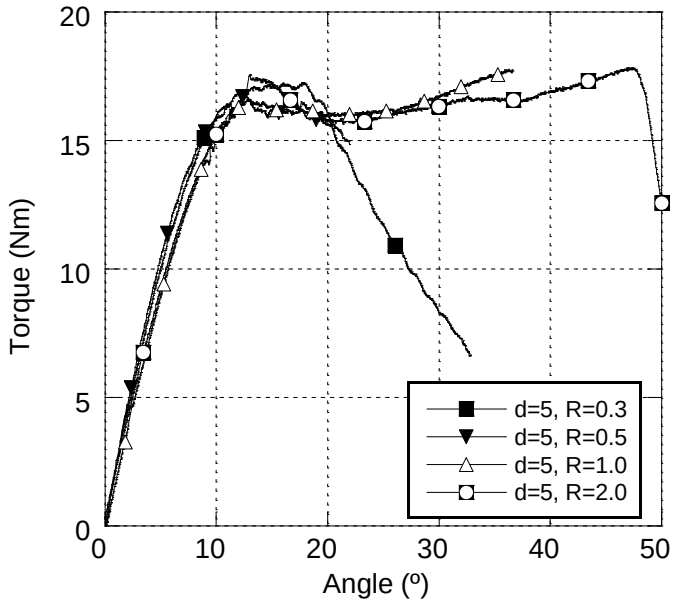

(a) U-notches

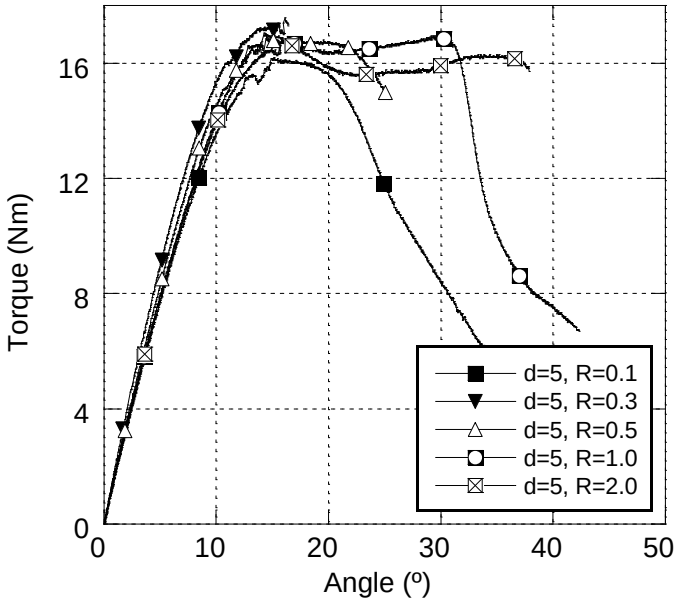

(b) V-notches

Figure 4.7: Experimental results obtained in the room temperature (20°C) torsion tests for a) U-notched specimens, b) V-notched specimens (d = 5 mm).

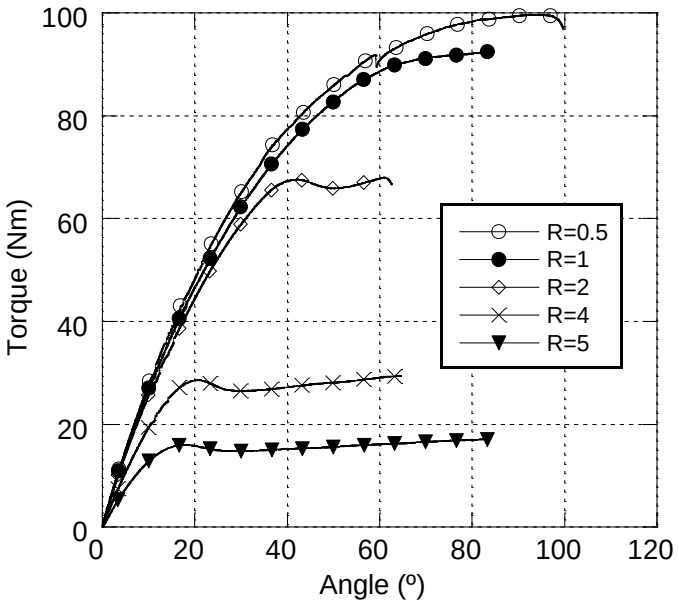

Figure 4.8: Experimental results obtained in the room temperature (20°C) torsion tests for semicircural-notches specimens.

4.4 Low Temperature Tests Results

Torque versus angle (with 25 mm gauge length) curves obtained at -60°C are plotted in Figs. 4.9, 4.10, 4.11 . For the sake of simplicity and given the repeatability of the results, only one single curve for each geometry is provided.

Previous tests on three point bending tests had shown an almost linear elastic behaviour up to failure [25, 29]. A similar behaviour was expected on these torsion tests. However, although the temperature decrease makes the specimens behavior considerably more brittle in terms of failure angles, it can be noticed how the curves show a clear non linear shape from their beginning, independently of the type of notch geometry.

Unlike in the case of the room temperature tests, the maximum torque which each specimen type is able to withstand is clearly dependent on the notch tip radius. In opinion of the author, this result suggests that failure is primarily governed by the stress concentration at the notch tip. Although the decrease of temperature was not been able to "linearize" the specimens behavior, it succeeded in the purpose of concentrating all the damage and failure mechanisms at the notch tip.

In Fig. **??**, torque versus angle (again with 25 mm gauge length) curves for plain cylinder and cracked specimens are plotted.

Some examples of failures patterns are shown in Fig. 4.13.

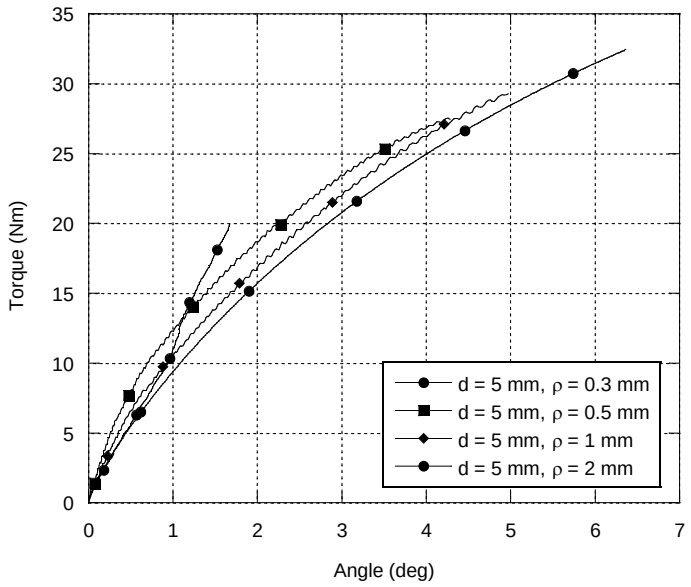

(a) U-notches

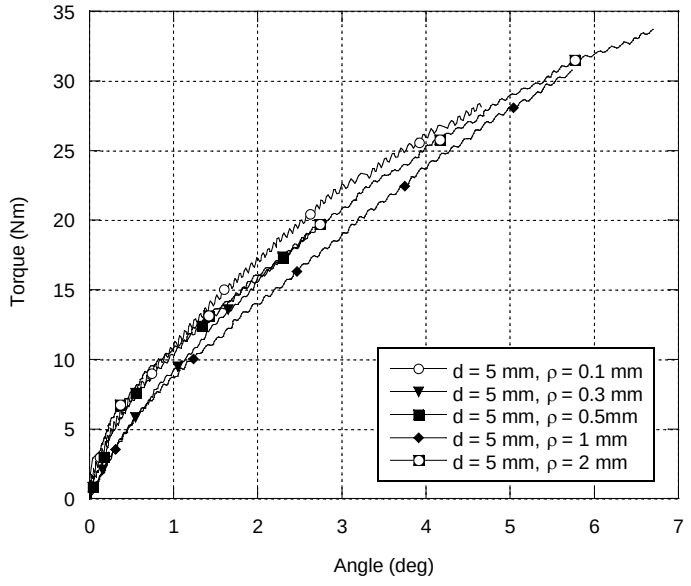

(b) V-notches

Figure 4.9: Experimental results obtained in the low temperature (-60°C) torsion tests for a) U-notched specimens, b) V-notched specimens (d = 5 mm).

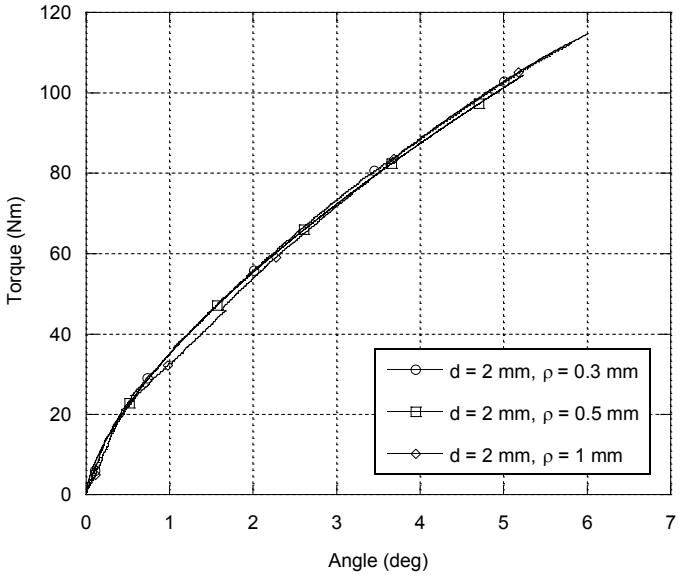

(a) U-notches

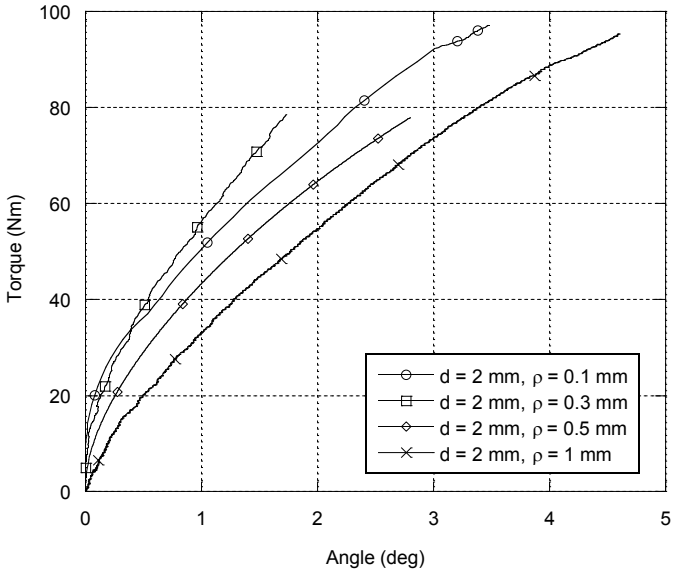

(b) V-notches

Figure 4.10: Experimental results obtained in the low temperature (-60°C) torsion tests for a) U-notched specimens, b) V-notched specimens (d = 2 mm).

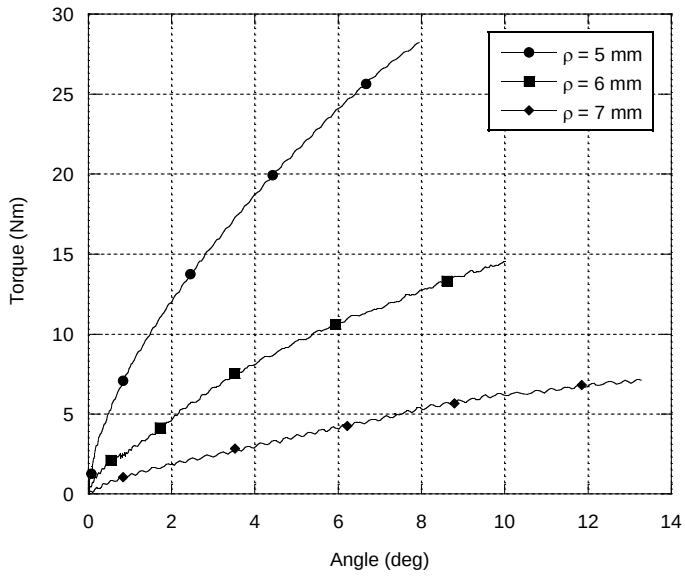

Figure 4.11: Experimental results obtained in the low temperature (-60°C) torsion tests for semicircural-notched specimens.

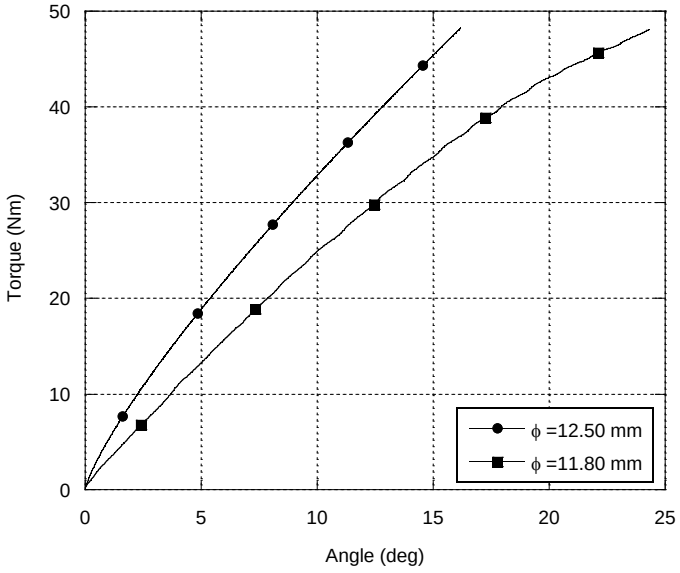

(a) U-notches

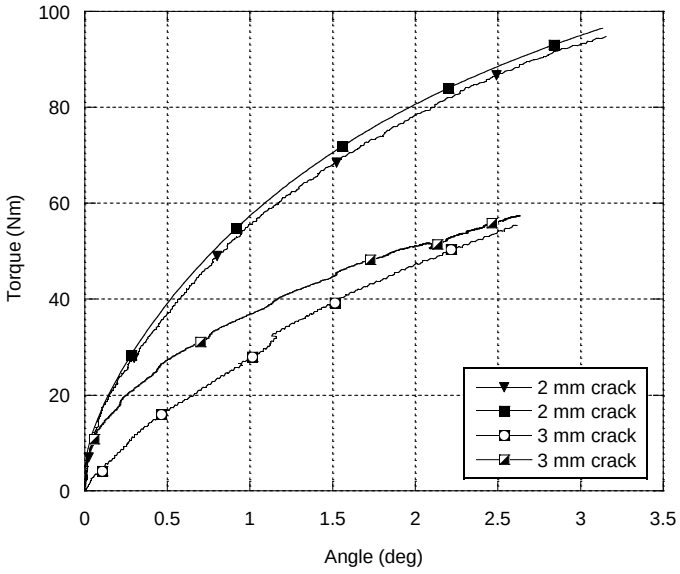

(b) plain specimens

Figure 4.12: Experimental results obtained in the low temperature (-60°C) torsion tests for a) plain specimens and b) cracked specimens (crack length a = 2 - 3 mm).

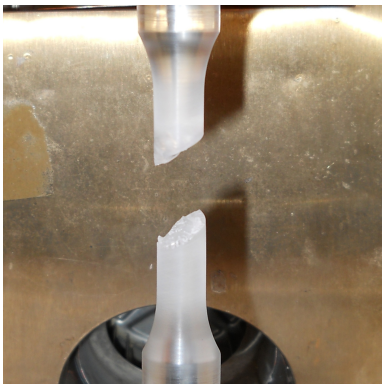

(a) plain specimen

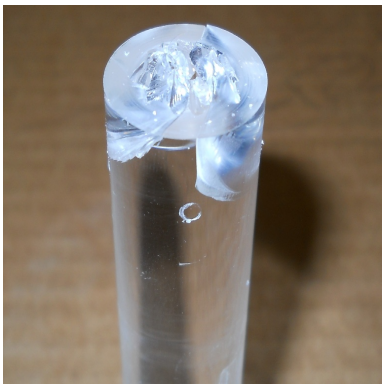

(b) U-notch specimen

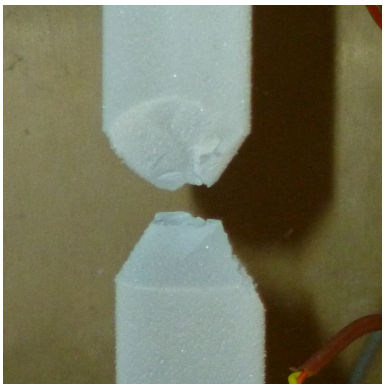

(c) V-notch specimen

(d) Semicircular-notch specimen

Figure 4.13: Failure exemples.

4.5 Stress-Strain curve in a non-linear torsion case

As shown in Sec. 4.4, PMMA behavior under torsion loading (Mode III) at -60º is totally different from its behavior under mode I or mode II test conditions (Gomez 2005; Berto 2007,2008). In torsion loading case, PMMA presents a completely non-linear behavior from the very beginning of the loading process. Under torsion loading, a linear relationship between the deformation and the distance of the point considered to the central axis is usually assumed. If the constitutive equation of the material were linear, then the relationship between the stress and the distance to the axis would be also linear. Such linear relationship can be expressed through Coulomb equation:

$$\tau = \frac{M_t}{J_p} r \tag{4.1}$$

where M_t is the applied torque, Jp is the polar intertia moment and r is the radius. Since the behaviour of PMMA at low temperature under torsion loading exhibited a non-linear behaviour, expression (4.1) is no longer valid and an alternative procedure to measure the material shear properties had to be devised.

One alternative could be to test under torsion a hollow cylinder with a very thin thickness. Due to the reduced thickness of the piece, the stress τ can be assumed to be constant in every point of the specimen, for each value of the applied torque M_t. However such test presents important practical difficulties related with geometrical instabilities and buckling of the walls of the cylinder. So we followed the idea that it is possible to obtain the desired geometry (pipe) by subtracting a cylinder with a diameter d from another cylinder with a bigger diameter D, i.e. $t = D - d$, where t is the thickness of the hollow cylinder (Figs. 4.14, 4.15), which must be as small as possible.

For that purpose we tested couples of plain cylinder (unnotched) specimens, the first one with a diameter $D = 12.50$ mm and the second one with a diameter $d = 11.80$ mm. Once we tested each couple of specimens, we subtracted the second specimen "Torque-Angle" curve (*System 2*) from the first one (*System 1*). So we obtained an equivalent hollow cylinder curve (Fig. 4.16). That equivalent hollow cylinder has a thickness $t = 0.7$ mm. In a equivalent system like that, we can consider a constant stress trade in the whole section for each value of the applied torque, by the relation:

$$\tau = \frac{M_t}{2\pi t r^2} \tag{4.2}$$

Again with the special devices described in the experimental tests section, we got the shear angle, γ, suffered by the specimens with a 25 mm gauge length. The τ-γ (torsion stress-strain) curve obtained is plotted in Fig. 4.17 (for the sake of simplicity, only one curve is shown). The maximum torsion stress value is $\tau_t = 153.5$ MPa.

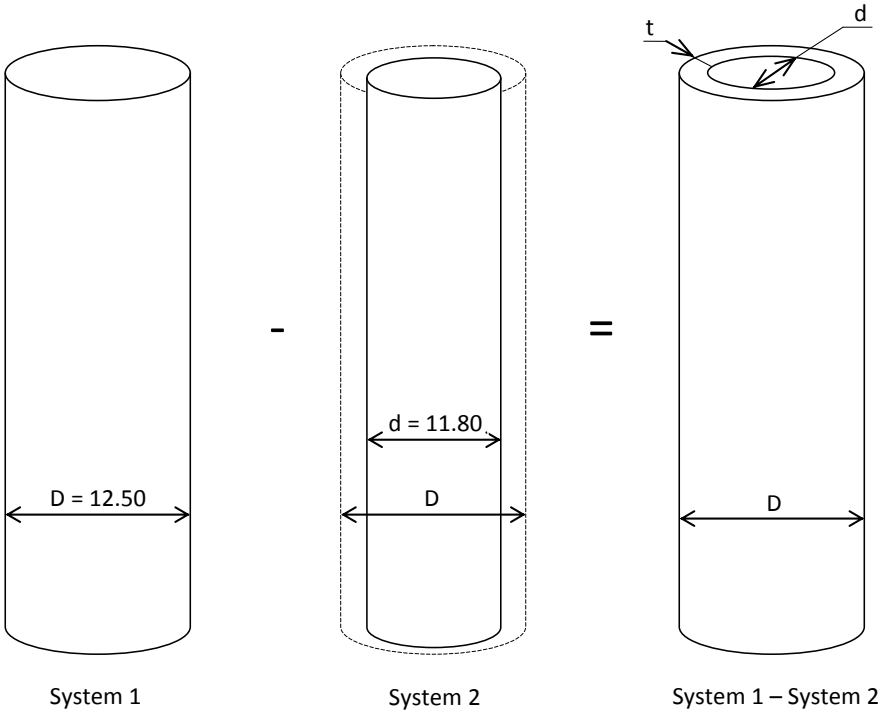

Figure 4.14: By subtracting a cylinder with a diameter d from another cylinder with a bigger diameter D, we can obtain a hollow cylinder with a thickness $t = D - d$.

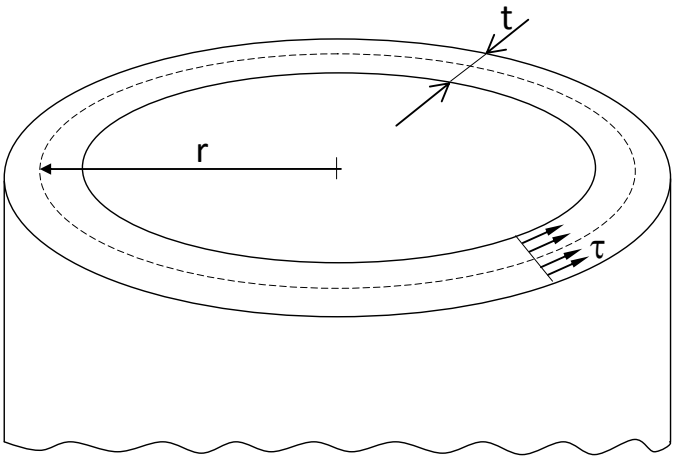

Figure 4.15: In a hollow cylinder (pipe) we can consider a constant stress trade (τ) in the whole thikness.

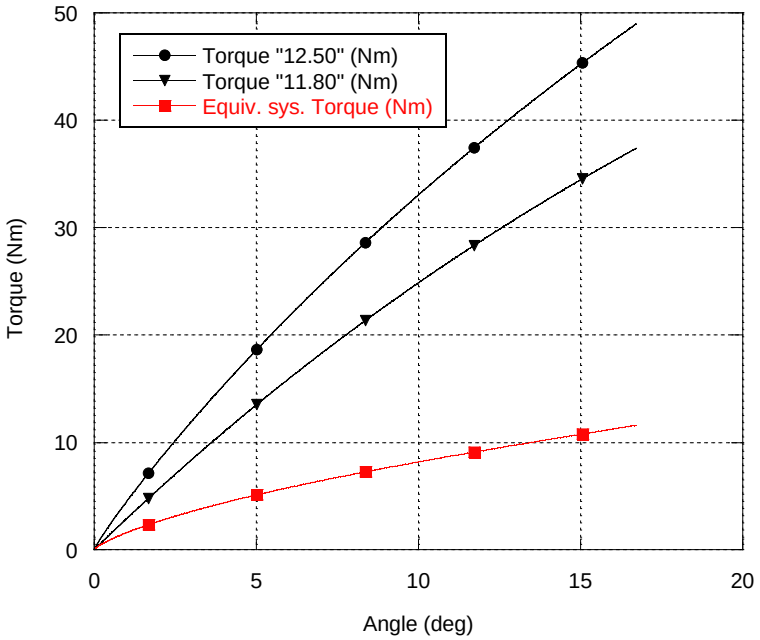

Figure 4.16: "Torque-Angle" specimens' curves and equivalent "Torque-Angle" pipe's curve.

By integrating the curve shown in Fig. 4.17, we can calculate the strain energy density. We can find the function $\tau(\gamma)$ by using a power fitting approximation. The strain energy density W_{eq} results:

$$W_{eq} = \int_0^{\gamma_{max}} \tau(\gamma)\, d\gamma \simeq 7 \text{ MPa} \tag{4.3}$$

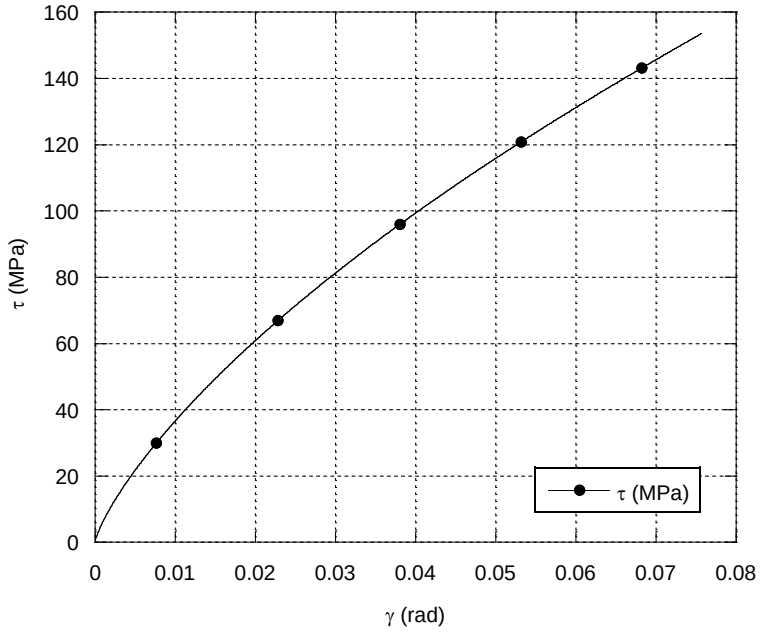

Figure 4.17: Torsion "Stress-Strain" curve obtained for PMMA at -60°C with the "equivalent-pipe method".

Chapter 5

Numerical Analysis Results

In the case of blunt notches, such as U or V notches, the stress intensity diminishes and the theory of the classical Linear Elastic Fracture Mechanics approach cannot be applied. The *Strain Energy Density* (SED) criterion aims to assess failure induced by notches in brittle materials. According to this approach, failure arises when the mean value of the strain energy density in a certain volume around the notch tip reaches a given threshold value, W_{3c}. Such volume is defined, in 2D geometries, by a circular area of constant thickness R_{3c}, named control radius.

The main advantage of this approach is that R_{3c} and W_{3c} are assumed to be a material property that can be obtained from standard characterization mechanical tests and thus they are not dependent on the notch geometry.

The expression of R_c for mode III (specimens under torsion), given by Eq. (3.1) is reported here for the sake of semplicity:

$$R_{3c} = \left(\sqrt{\frac{e_3}{1+\nu}} \cdot \frac{K_{3c}}{\tau_t} \right)^{\left(\frac{1}{1-\lambda_3}\right)} \tag{5.1}$$

The critical energy value can be obtained from the maximum shear strength τ_t by Beltrami's expression (3.3):

$$W_{3c} = \frac{\tau_t^2}{2G} \tag{5.2}$$

where G is the shear modulus. In Tab. 5.1 are shown the values of K_{3c} and τ_t, from the experimental tests and of R_{3c} and W_{3c}, found by applying the values from Tab. 3.1 to Eqs. (5.1) and (5.2). The values are given for both room [35, 37] and low temperature cases: Comparing the control radius obtained from the torsion tests with the value

Table 5.1: Mode III experimental and critical values.

	Room Temperature	**Low Temperature**
K_{3c} (MPa$\sqrt{\text{m}}$)	3.35	5.97
τ_t (MPa)	73.46	153.50
R_{3c} (mm)	0.61	0.45
W_{3c} (MJ/m^3)	3.4	6.5

obtained by Berto et al. in [29], we can note that the volume radius under torsion

(Tab. 5.1) results to be much grater than the one found under tensile loading (equal to $R_c = 0.035$ mm). Under torsion loads a number of nonlinear effects were detected resulting in a control volume dependent on the loading mode.

Finite Element simulations were performed for each notch geometry assuming linear elastic material (with the mechanical properties shown in Tab. 4.1). Actually, we can note that the energy density experimental value (Sec. 4.5) and the theoretical elastic one (found by using (5.2)) are very close. Therefore, the choose of a linear elastic approach is justified. We toke benefit from the linearity being able to make faster simulations than using an elastic-plastic model.

The numerical values of SED W_{ref} were calculated numerically inside the critical radius region for a torque of 1 Nm, by using the FE code ANSYS 13.0©. All the analyses were carried out by using eight-node harmonic elements (plane 83) under axial-symmetric conditions. Only one quarter of the geometry has been modelled in the positive quadrant. Being the SED value substantially mesh insensitive [30, 32], we used a free mesh for all models. There is no need to assure the similarity among the meshes used to model different geometries. Attention should be paid only to the correct definition of the control volume according to Fig. 5.1.

Taking benefit from the linearity of the approach, we calculated the average strain energy density within the critical region for each tested specimen through:

$$W = M_{max}^2 \cdot W_{ref} \tag{5.3}$$

Where M_{max} is the actual maximum torque for the specimen considered and W is the average strain energy density calculated for that actual specimen.

Once found the strain energy density for each tested specimen, we can calculate the theoretical value of the failure torque M_{th}, by using the relation: $\sqrt{W/W_c} = M_{max}/M_{th}$. The comparison between theoretical and experimental values of the maximun load and the value of SED for each test, are shown in Tabs. 5.2, 5.3, 5.4, 5.5.

The results are also given in graphical form in Figs. 5.3, 5.4, 5.5, 5.2 where the experimental values of the critical loads (open diamonds) have been compared with the theoretical predictions based on the constancy of SED in the control volume (open squares). The plots are given for the notched PMMA specimens as a function of the notch radius ρ for U, V and semicircular[1] notches and as a function of crack length (a) for cracked specimens (Fig. 5.2)[2].

The theoretically predicted loads are in agreement with the experimental results, wich lay, exept for few ones, in a ±20% scatter band. Scatters higher than ±20% are probably due to non-linear behaviour of the material or to an incorrect specimens

[1]For semicircular norches specimens the critical energy value is different, because those specimens were made with a different kind of PMMA material. See [37], for the properties and the charaterization of that material.

[2]See Appendix B for a comparison with room temperature results

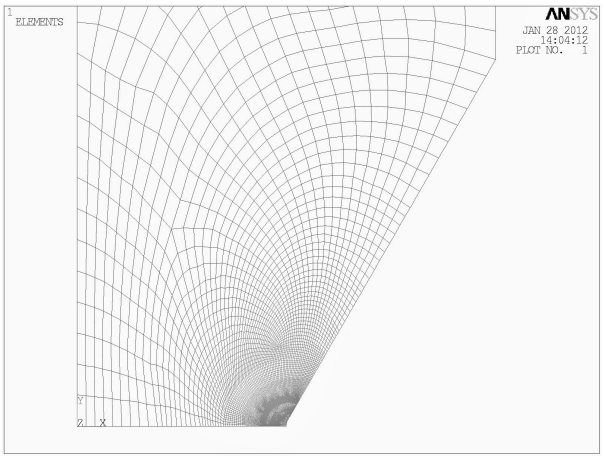

(a) Mesh

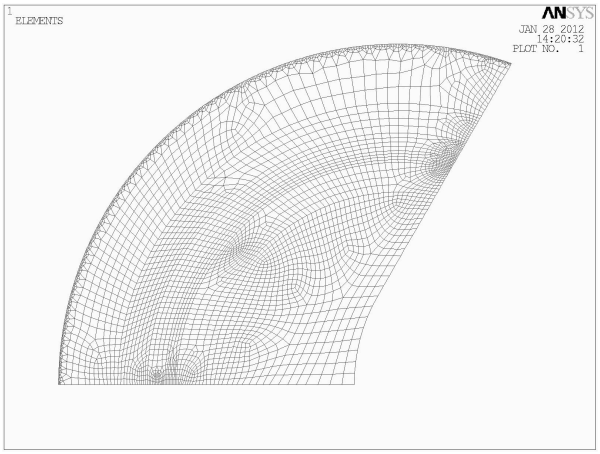

(b) Control Volume

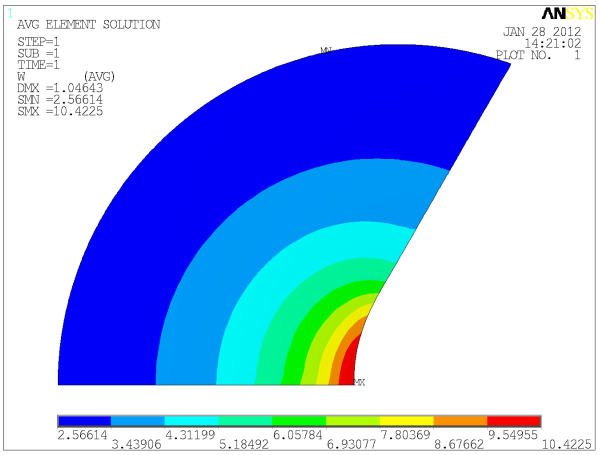

(c) Average SED

Figure 5.1: a) Mesh, b) control volume and c) iso-strain energy density contour lines, for a V-notch with: $2\alpha = 120^{o}$, $\rho = 0.3$ mm, d = 5 mm.

Table 5.2: Compairson between theoretical and experimental torque to failure and values of average SED (W) for cracked specimens

a (mm)	M_{max} **(Nm)**	M_{th} **(Nm)**	**%**	**W (MJ/m^3)**
3	57.37	62.08	-7.58	7.62
3	54.53	62.08	-12.16	5.55
3	60.95	62.08	-1.81	5.02
3	64.82	62.08	4.42	6.27
2	94.80	92.10	2.93	7.01
2	96.51	92.10	4.78	7.26

Table 5.3: Compairson between theoretical and experimental torque to failure and values of average SED (W) for U-notched specimens

d (mm)	ρ **(mm)**	M_{max} **(Nm)**	M_{th} **(Nm)**	**%**	**W (MJ/m^3)**
5	0.3	17.95	25.34	-29.18	4.03
	0.3	22.65	25.34	-10.63	5.19
	0.3	19.97	25.34	-21.21	4.04
	0.5	26.14	25.32	3.23	6.93
	0.5	27.31	25.32	7.85	7.56
	0.5	27.47	25.32	8.48	7.65
	1	29.31	26.26	11.60	8.33
	1	29.80	26.26	13.47	8.61
	1	30.56	26.26	16.36	9.05
	2	31.36	27.64	13.47	8.37
	2	30.79	27.64	11.41	8.07
	2	32.36	27.64	17.09	8.94
2	0.3	114.79	92.39	24.25	9.08
	0.3	112.21	92.39	21.46	8.68
	0.3	90.89	92.39	-1.62	5.59
	0.5	104.15	92.62	12.45	7.49
	0.5	115.15	92.62	24.32	9.25
	0.5	114.94	92.62	24.09	9.25
	1	124.65	95.09	31.09	10.05
	1	76.24	95.09	-19.82	4.10
	1	114.69	95.09	20.62	8.87

Table 5.4: Compairson between theoretical and experimental torque to failure and values of average SED (W) for V-notched specimens

d (mm)	**ρ (mm)**	**M_{max}** (Nm)	**M_{th}** (Nm)	**%**	**W (MJ/m^3)**
5	0.1	29.06	26.04	11.61	8.10
	0.1	31.79	26.04	22.09	9.67
	0.1	19.02	26.04	-26.95	3.34
	0.1	22.43	26.04	-13.85	4.83
	0.1	28.16	26.04	8.15	4.53
	0.3	20.30	26.00	-21.93	3.96
	0.3	18.60	26.00	-28.47	3.89
	0.3	19.10	26.00	-26.54	3.73
	0.3	24.24	26.00	-6.77	5.65
	0.3	22.31	26.00	-14.20	5.23
	0.5	18.68	26.02	-28.21	3.51
	0.5	19.20	26.02	-26.22	3.54
	0.5	19.73	26.02	-24.18	3.74
	0.5	19.95	26.02	-23.33	3.82
	0.5	20.23	26.02	-22.26	4.19
	1	31.59	26.21	20.54	9.45
	1	32.64	26.21	24.55	10.09
	1	30.79	26.21	17.49	8.98
	2	31.39	26.95	16.48	8.82
	2	33.70	26.95	25.05	9.97
	2	31.63	26.95	17.37	8.98
2	0.1	93.87	94.35	-0.51	6.44
	0.1	122.52	94.35	29.86	10.96
	0.1	98.67	94.35	4.58	7.11
	0.3	94.19	94.58	-0.42	6.45
	0.3	79.39	94.58	-16.06	4.58
	0.3	78.52	94.58	-16.98	4.48
	0.5	73.91	94.98	-22.19	3.94
	0.5	77.94	94.98	-17.94	4.38
	0.5	80.31	94.98	-15.45	4.65
	1	95.31	96.37	-1.10	6.36
	1	102.82	96.37	6.70	7.43
	1	124.65	96.37	29.35	10.88

Table 5.5: Compairson between theoretical and experimental torque to failure and values of average SED (W) for semicircular notched specimens

ρ (mm)	M_{max} (Nm)	M_{th} (Nm)	%	W (MJ/m^3)
5	30.30	29.94	1.21	6.66
5	28.22	29.94	-5.74	5.78
5	28.39	29.94	-5.17	5.85
6	15.21	16.19	-6.06	5.74
6	14.53	16.19	-10.26	5.24
6	15.77	16.19	-2.60	6.17
7	7.12	7.27	-2.04	6.24

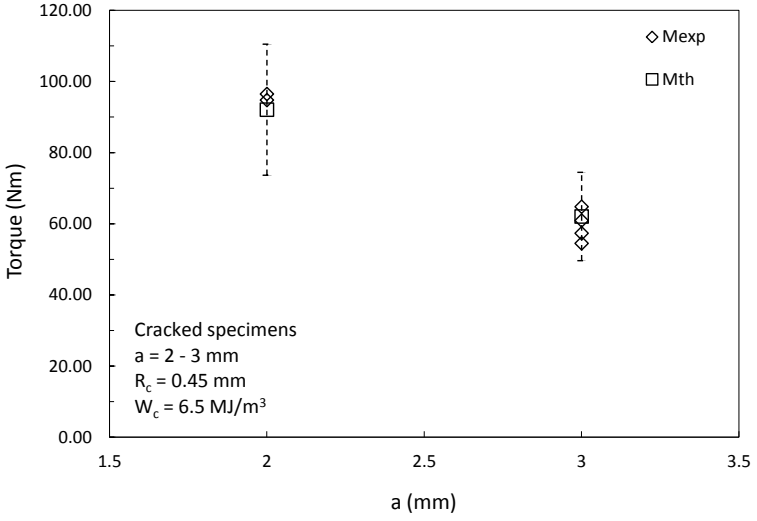

Figure 5.2: Comparison between experimental data and theoretical assessment (M_{th} - open squares) for the PMMA cracked specimens.

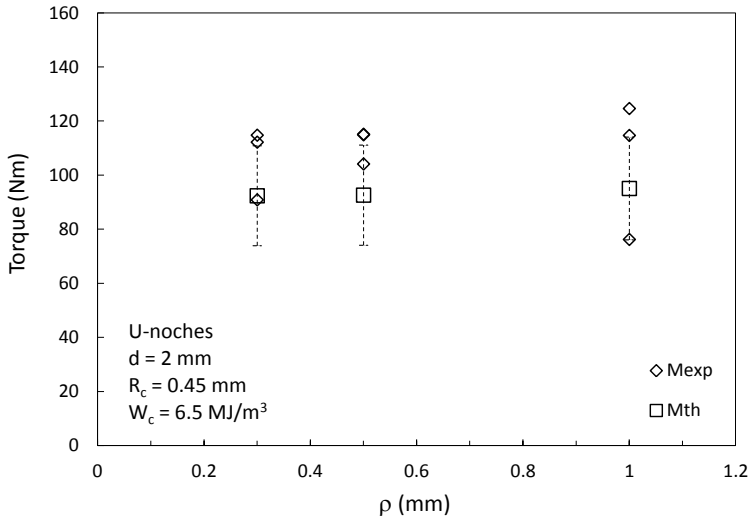

(a) U-noches

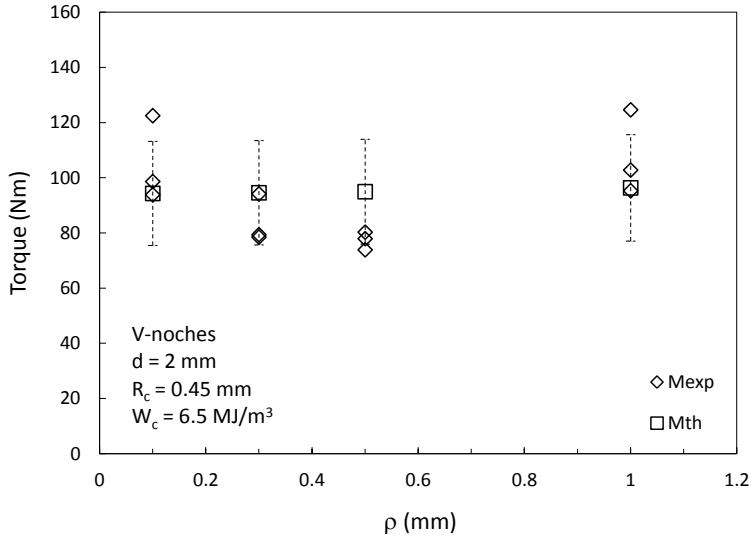

(b) V-noches

Figure 5.3: Comparison between experimental data and theoretical assessment (M_{th} - open squares) for the PMMA specimens; a) U-shaped and b) V-shaped notches specimens, with d = 2 mm.

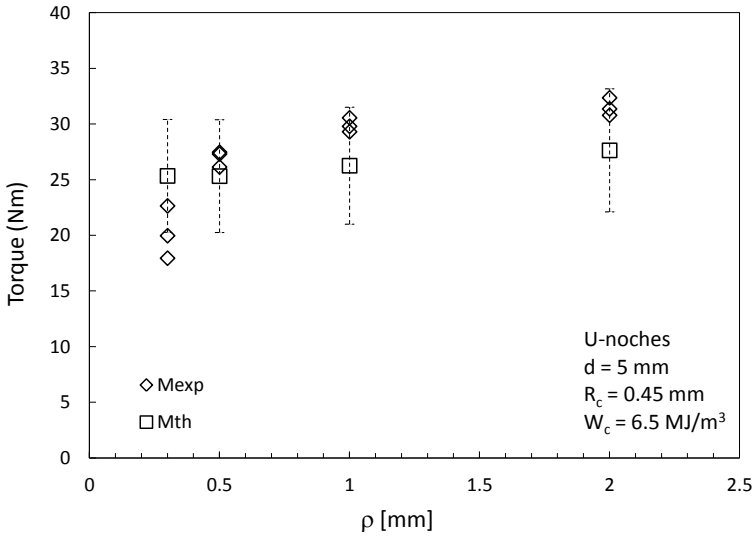

(a) U-noches

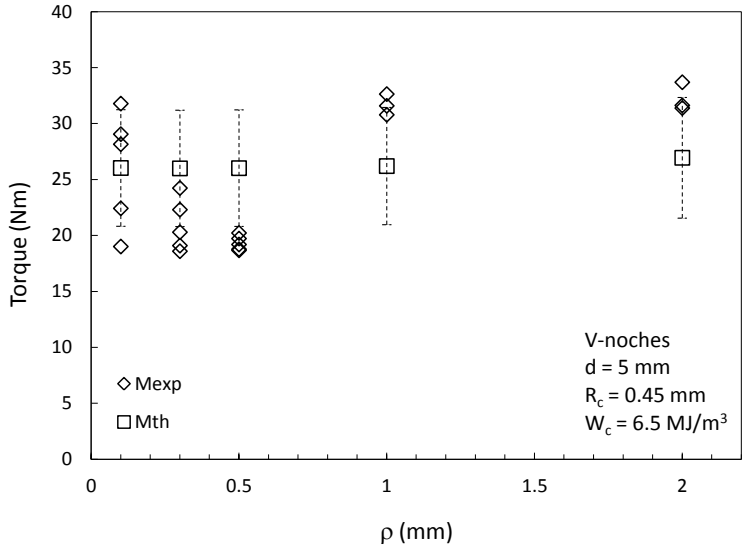

(b) V-noches

Figure 5.4: Comparison between experimental data and theoretical assessment (M_{th} - open squares) for the PMMA specimens; a) U-shaped and b) V-shaped notches specimens, with d = 5 mm.

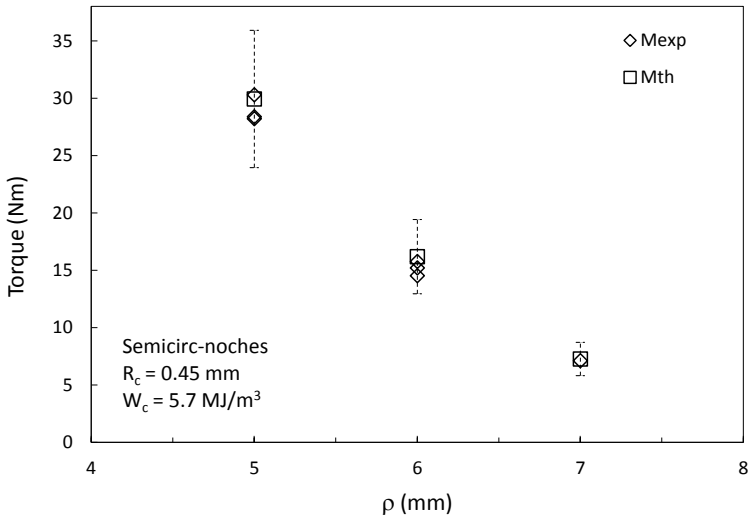

Figure 5.5: Comparison between experimental data and theoretical assessment (M_{th} - open squares) for the PMMA semiciruclar notched specimens.

machining, wich lead up to "unconventional" failures (i.e. not so close to the notch tip - Fig. 5.6).

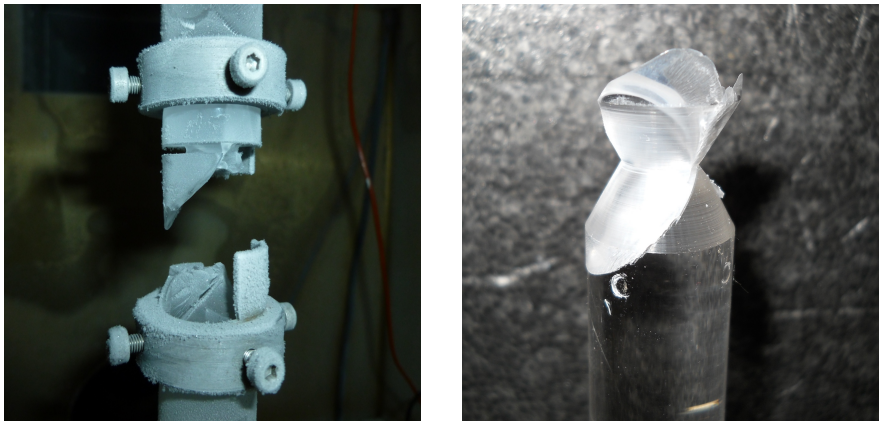

(a) U-noches (b) V-noches

Figure 5.6: Bad failures for a) a U-notched specimen and b) a V-notched specimen.

In Fig. 5.7 is shown a synthesis in terms of the square root value of the local energy averaged over the control volume of radius R_c, normalised with respect to the critical energy of the material (dividing the values by W_c), as a function of the ratio ρ/R_c. The ratio on the vertical axis is proportional to the fracture load. The aim is to investigate the range of accuracy of all SED-based fracture assessments for the tested PMMA specimens. From the figure, it is clear that the scatter of the data is limited and independent of the notch opening angle. We can observe how in both cases of room and low temperature results, almost all the normalized average SED values move within

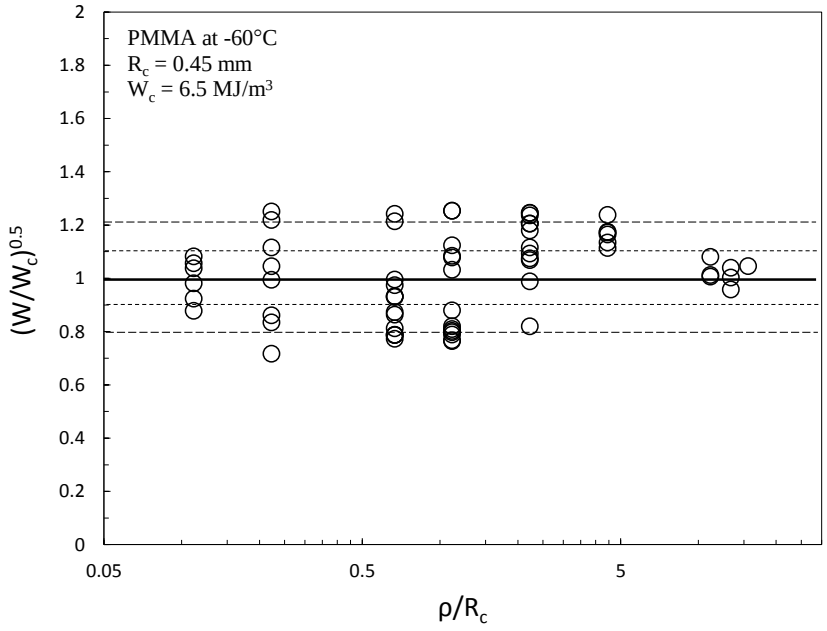

(a) low temperature

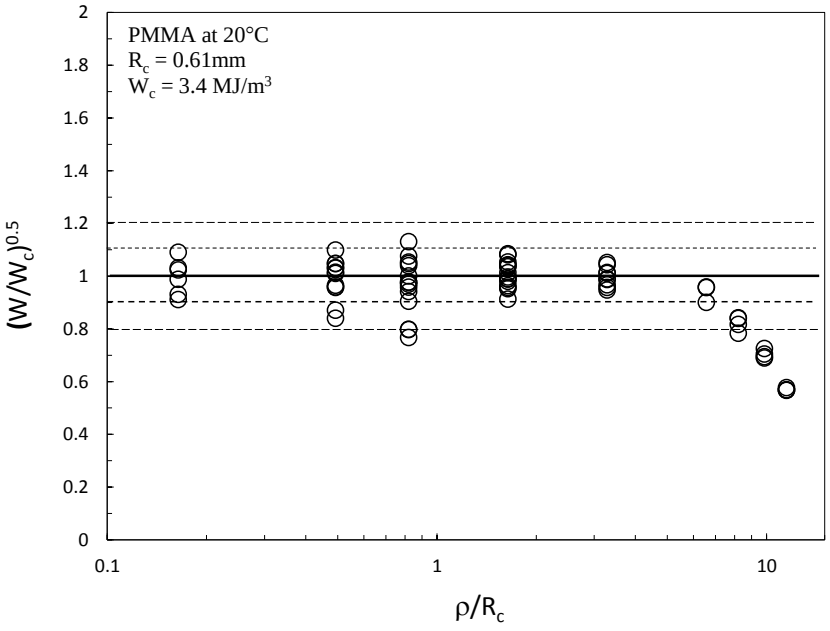

(b) room temperature

Figure 5.7: Synthesis based on SED of the torsion tests results at a) low temperature and at b) room temperature.

the 1±20% value. However, in the case of the room temperature, values corresponding to big notch radius (semicircular ones) lay completely outside this interval. That result suggests that while at low temperatures material nonlinearities are concentrated close to the notch tip, fulfilling thus the assumptions on which the SED criterion is based, as the temperature increases, nonlinearities extend beyond this region and therefore this kind of criterions based on an autonomous region loses accuracy.

The degree in which the SED criterion is fulfilled, is reflected by the way in which the normalized average strain energy values W/W_c are close to 1, no matter which notch tip radius we have. This means that in both cases there is no "radius effect". The scatter is more or less homogeneus through all the studied radii.

Chapter 6

Conclusions

Fracture behaviour of PMMA under torsion loading was investigated experimentally and theoretically using axisymmetric specimens weakened by sharp and blunt-tip (U, V and semicircular) notches. PMMA specimens were tested by comparing room and low temperature (-60°C) behaviour.

Common engineering practice requires the machining on many pieces of some details such as holes, U-notches, V-notches, etc. that act as stress concentrators, although they are intentionally included in the piece. As stress concentrators they can lead to a premature and unforeseen catastrophic failure of a structure. Despite these kind of defects are relatively common, the knowledge achieved by Fracture Mechanics about them is considerably less than the knowledge about theoretical cracks.

To the best of author's knowledge, the amount of data available in the literature about notch specimens under torsion is limited. For this reason, the purpose of this work was twofold. First, a new set of experimental data from notched samples made of PMMA was presented with different values of notch opening angles, root radii and notch geometries (U, V and semicircular), which should be useful to engineers engaged with static strength analysis of PMMA components. Second, a fracture criterion was applied to the torsion loading case. This criterion is based on the strain energy density (SED) averaged over a well-defined control volume surrounding the notch tip. Since at room temperature the stress-strain behaviour of the material under torsion loading conditions was far from being linear elastic, tests were focused at -60°C.

The present work would extend what was made in [25, 29, 35] for in-plane tension-shear loading conditions in notched PMMA specimens. However the material behaviour under torsion loading was very different with respect to mixed mode (I+II) loading conditions [29]. The control radius and strain energy density values for mixed mode (I+II) loading conditions are, respectively, $R_c = 0.035$ mm and $W_c = 1.6$ MJ/m^3 [29]. In the torsion loading case we found, respectively, $R_{3c} = 0.45$ mm and $W_c = 6.5$ MJ/m^3. The difference is due to the different stress concentrations between the two different loading modality. Stress concentrations are bigger in the case of torsion loading. Therefore, PMMA seems to present a loading condition-dependent behaviour.

Good matching was found between the experimental data related to the critical loads

to failure and the theoretical assessments based on the constancy of the mean SED over the material-dependent control volume. From the agreement between the theoretical and experimental results, it can be deduced that for the PMMA the torsion critical energy and the radius of the control volume are both material properties influenced by loading conditions, but not influenced by the geometrical parameters.

The author suggests more torsion tests on notched specimens and torsion tests on unnotched specimens (by using the "equivalent system" method – see Sec. 4.5) for a better material characterization under torsion loading. Furthermore, with the aim to improve the mode III fracture toughness investigation, it would be useful to make some low temperature tearing tests on PMMA cracked plates, by using, for example, the method of anti-clastic plate bending (ACPB) or equivalently the plate twist method as Farshad and Flueler described in [15].

Ringraziamenti

Vorrei ringraziare prima di tutti il dott. Filippo Berto per aver reso possibile il lavoro descritto in queste pagine, per la sua disponibilità e per quello che mi ha trasmesso in questi mesi in cui ho avuto la possibilità di lavorare con lui.

Voglio ringraziare con tutto il cuore il prof. David Cendón per la disponibilità, la pazienza e la simpatia dimostratami e per tutto quello che mi ha insegnato durante il mio lavoro a Madrid e ringrazio infinitamente il prof. Manuel Elces per l'accoglienza dimostratami. Un grazie anche ai raggazzi dell'officina meccanica per l'aiuto che mi hanno sempre dato e ai ricercatori e professori del Dipartimento di Scienza dei materiali della UPM.

Grazie a Damiano, Nico, Jacopo e Valentina per aver condiviso i momenti di studio (e non...). Ringrazio tutti gli amici (non servono i nomi, loro sanno chi sono). Ancora un grazie a Nicolò per le correzioni di forma durante la stesura.

Un ringraziamento particolare va a Emmanuele Zambon per le dritte e i consigli preziosi che mi ha dato per la stesura di questa tesi.

Ringrazio Luigi Sella per aver sempre avuto le parole giuste al momento giusto.

Ultimi, ma sicuramente non ultimi, vorrei ringraziare i miei genitori per il supporto datomi e per avermi sopportato durante il corso di tutta la mia vita!

Dedico il presente lavoro di tesi a mia nonna Marcella, essendole per sempre grato di tutto quello che ci ha dato.

Vicenza, 25 ottobre 2012

Bibliography

[1] Neuber H; *Kerbspannungslehre, 2*; Springer-Verlag, Berlin, 1958.

[2] Bazaj DK, Cox EE; *Stress concentration factors and notch sensitivity of graphite* Carbon 1969; 7(6): 689–97.

[3] Gross R, Mendelson A; *Plane Elastostatic Analysis of V-Notched Plates*; International Journal of Fracture Mechanics 1972; 10:305–321.

[4] Sih GC; *Aspecial theory of crack propagation* In: Sih GC (ed) Methods of analysis and solutions of crack problems; Noordhoff, International Publishing 1973, Leyden, pp 21–45.

[5] Sih GC; *Strain-Energy-Density factor applied to mixed mode crack problems*; Int J Fracture 1974; 10: 305–321.

[6] Glinka G.; *Energy density approach to calculation of inelastic strain-stress near notches and cracks*; Eng Fract Mech 1985; 22: 485–508.

[7] Neuber H; *Kerbspannungslehre, 3*; Springer-Verlag, Berlin, 1985.

[8] Kawakami H *Notch sensitivity of graphite materials for VHTR* J Atomic Energy Soc Jpn 1985;27(4):357–64.

[9] Sih GC; *Mechanics of fracture initiation and propagation: surface and volume energy density applied as failure criterion*; Kluwer Academic Publisher, Dordrecht, 1991.

[10] Seweryn A; *Brittle fracture criterion for structures with sharp notches*; Engineering Fracture Mechanics 1994; 47, 673–681.

[11] Anderson T L; *Fracture Mechanics* 2nd ed; CRC press, 1995; pp. 33,

[12] Seweryn A, Poskrobko S, Mróz Z; *Brittle fracture in plane elements with sharp notches under mixed-mode loading*; Journal of Engineering Mechanics 1997; 123, 535–543.

[13] Qian J, Hasebe N; *Property of eigenvalues and eigenfunctions for an interface V-notch in antiplane elasticity*; Eng Fract Mech 1997; 56: 729–34.

[14] Elices M; *Mecánica de la Fractura Aplicada a Sólidos Elásticos Bidimensionales*; ETS de Ingenieros de Caminos, Canales y Puertos, Universidad Politécnica de Madrid, 94 pp., Madrid, Spain, 1998.

[15] Farshad M, Flüeler P; *Investigation of mode III fracture toughness using an anti-clastic plate bending method*; Engineering Fracture Mechanics 1998, 60: 597-603.

[16] Lazzarin P, Zambardi R; *A finite-volume-energy based approach to predict the static and fatigue behaviour of components with sharp V-shaped notches*; Int J Fracture 2001; 112: 275–298.

[17] Filippi S, Lazzarin P, Tovo R; *Developments of some explicit formulas useful to describe elastic stress fields ahead of notches in plates*; International Journal of Solids and Structures 2002; 39, 4543-4565.

[18] Seweryn A, Lukaszewicz A; *Verification of brittle fracture criteria for elements with V-shaped notches*; Engineering Fracture Mechanics 2002; 69, 1487–1510.

[19] Lazzarin P, Lassen, T, Livieri P; *A Notch Stress Intensity approach applied to fatigue life predictions of welded joints with different local toe geometry*; Fatigue and Fracture of Engineering Materials and Structures 2003; 26, 49–58.

[20] Lazzarin P, Sonsino C M, Zambardi R; *A Notch Stress Intensity approach to predict the fatigue behaviour of T butt welds between tube and flange when subjected to in–phase bending and torsion loading*; Fatigue and Fracture of Engineering Materials and Structures 2004; 27: 127–141.

[21] Gearing B P, Anand L; *Notch-sensitive fracture of polycarbonate*; Int J of Solids and Structures 2004; 41: 827–845.

[22] Yosibash Z, Bussiba Ar, Gilad I; *Failure criteria for brittle elastic materials*; Int J Fract 2004; 125: 307–333.

[23] Eppley B L; *Biomechanical testing of alloplastic PMMA cranioplasty materials*; J Craniofac Surg 2005; 16(1): 140-3.

[24] Frazer R Q, Byron R T, Osborne P B, West K P; *PMMA: an essential material in medicine and dentistry*; J Long Term Eff Med Implants 2005; 15(6):629-39.

[25] Gómez F J, Elices M, Planas J; *The Cohesive Crack Concept: application to PMMA at -60^oC*; Eng. Fract. Mech. 2005; 72: 1268-1285.

[26] Lazzarin P, Berto F; *Some expressions for the strain energy in a finite volume surrounding the root of blunt V-notches*; Int J Fracture 2005; 135: 161–185.

[27] Livieri P, Lazzarin P; *Fatigue strength of steel and aluminium welded joints based on generalised stress intensity factors and local strain energy values*; Int J of Fracture 2005; 133: 247–276.

[28] Yasin S, Khalid M N, Hasko D G, Sarfraz S; *Correlation of surface roughness with edge roughness in PMMA resist*; Microelectronic Engineering 2005; 78–79: 484-489.

[29] Berto F, Lazzarin P, Gomez F J, Elices M; *Fracture assessment of U-notches under mixed mode loading: two procedures based on the 'equivalent local mode I' concept*; Int J Fracture 2007; 148:415–33.

[30] Lazzarin P, Berto F, Gomez F J, Zappalorto M; *Some advantages derived from the use of the Strain Energy Density over a control volume in fatigue strength assessments of welded Joints*; Int J Fatigue 2008; 30:1345–57.

[31] Berto F, Lazzarin P; *A review of the volume-based strain energy density approach applied to V-notches and welded structures*; Theor Appl Fract Mech 2009; 52:183–94.

[32] Lazzarin P, Berto F, Zappalorto M; *Rapid calculations of Notch Stress Intensity Factors based on averaged Strain Energy Density from coarse meshes: theoretical bases and applications*; Int J Fatigue 2010; 32(10):1559-67.

[33] Berto F, Lazzarin P; *Fatigue strength of structural somponents under multi-axial loading in terms of local energy density averaged on a control volume*; Int J Fatigue 2011; 33(8):1055-65.

[34] Stefanescu E A, Tan X, Lin Z, Bowler N, Kessler M R; *Multifunctional fiberglass-reinforced PMMA-BaTiO3 structural/dielectric composites*; Polymer 52 2011; 2016-2024

[35] Berto F, Elices M, Lazzarin P, Zappalorto M; *Behavior of notched round bars made of PMMA subjected to torsion at room temperature*; Submitted to Engng Fract Mech 2012.

[36] Berto F, Lazzarin P, Ayatollahi M R; *Brittle fracture of sharp and blunt V-notches in isostatic graphite under torsion loading*; Carbon 2012. In press.

[37] Fioretto G, Cendón D A, Berto F, Lazzarin P, Elices M; *Fracture behaviour of notched round bars made of PMMA subjected to torsion at different temperatures*; In proceeding of the XXIX Spanish Structural Integrity Society conference, March 2012, Bilbao.

[38] Zulian P; *Componenti intagliati soggetti a modo misto: prove sperimentali e previsioni teoriche*; Università degli Studi di Padova, 2012, Padova.

Appendix A

Functions expressions and parameters values of Sec. 2.1

In this section are shown the expressions of the eigenfunctions and of the parameters used in Sec. 2.1.

A.1 Angular functions expressions

The angular functions f_{ij} and g_{ij} are given by [17]

$$\begin{Bmatrix} f_{\theta\theta} \\ f_{rr} \\ f_{r\theta} \end{Bmatrix} = \frac{1}{1+\lambda_1+\chi_{b_1}(1-\lambda_1)} \left(\begin{Bmatrix} (1+\lambda_1)\cos(1-\lambda_1)\theta \\ (3-\lambda_1)\cos(1-\lambda_1)\theta \\ (1-\lambda_1)\sin(1-\lambda_1)\theta \end{Bmatrix} + \right. \\ \left. + \chi_{b_1}(1-\lambda_1) \begin{Bmatrix} \cos(1+\lambda_1)\theta \\ -\cos(1+\lambda_1)\theta \\ \sin(1+\lambda_1)\theta \end{Bmatrix} \right) \tag{A.1}$$

$$\begin{Bmatrix} g_{\theta\theta} \\ g_{rr} \\ g_{r\theta} \end{Bmatrix} = \frac{q}{4(q-1)[1+\lambda_1+\chi_{b_1}(1-\lambda_1)]} \\ \cdot \left(\chi_{d_1} \begin{Bmatrix} (1+\mu_1)\cos(1-\mu_1)\theta \\ (3-\mu_1)\cos(1-\mu_1)\theta \\ (1-\mu_1)\sin(1-\mu_1)\theta \end{Bmatrix} \chi_{c_1} \begin{Bmatrix} \cos(1+\mu_1)\theta \\ -\cos(1+\mu_1)\theta \\ \sin(1+\mu_1)\theta \end{Bmatrix} \right) \tag{A.2}$$

A.2 Parameters

The values of the parameter used in Sec. 2.1 to calculate the Mode I stress distribution (2.1), the control radius (2.12) and the strain energy are shown in the following Tables [26]. In the first one, Tab. A.1, are reported the parameters for stress distributions, for some tipical angle[1]. In the second one, the integral I_1 (2.8) is given as a function of the notch angle (Tab. A.2).

[1] However, all of those parameters have a close form expression [17].

Table A.1: Parameters for stress distributions, Equations (2.1) and (2.14).

2α (rad)	q	λ_1	μ_1	χ_{b_1}	χ_{c_1}	χ_{d_1}	$\tilde{\omega}_1$
0	2	0.5	-0.5	1	4	0	1
$\pi/6$	1.8333	0.5014	-0.4561	1.0707	3.7907	0.0632	1.034
$\pi/4$	1.7500	0.5050	-0.4319	1.1656	3.5721	0.0828	1.014
$\pi/3$	1.6667	0.5122	-0.4057	1.3123	3.2832	0.096	0.970
$\pi/2$	1.5000	0.5448	-0.3449	1.8414	2.5057	0.1046	0.810
$2\pi/3$	1.3334	0.6157	-0.2678	3.0027	1.5150	0.0871	0.570
$3\pi/4$	1.2500	0.6736	-0.2198	4.1530	0.9933	0.0673	0.432
$5\pi/6$	1.1667	0.7520	-0.1624	6.3617	0.5137	0.0413	0.288

Table A.2: Integral I_1 for sharp V-notches, as a function of the notch angle and the Poisson coefficient.

2α (deg)	γ/π	λ_1	I_1		
			$\nu = 0.3$	$\nu = 0.35$	$\nu = 0.4$
0	1	0.5000	0.845	0.7425	0.6300
15	23/24	0.5002	0.8431	0.7416	0.6303
30	11/12	0.5014	0.8366	0.7382	0.6301
45	7/8	0.5050	0.8247	0.7311	0.6282
60	5/6	0.5122	0.8066	0.7194	0.6235
75	19/24	0.5247	0.7819	0.7026	0.6152
90	3/4	0.5445	0.7504	0.6801	0.6024
105	17/24	0.5739	0.7124	0.6519	0.5849
120	2/3	0.6157	0.6687	0.6184	0.5624
135	5/8	0.6736	0.6201	0.5796	0.5344
150	7/12	0.7520	0.5678	0.5366	0.5013
160	5/9	0.8187	0.5315	0.5058	0.4767
170	19/36	0.9000	0.4957	0.4755	0.4523

Appendix B

Experimental data and SED theoretical assessment at room temperature

In this section are reported the figures obtained by data from [35, 37, 38]. Those figures show the comparison between experimental data and theoretical assessment for the PMMA (cracked and notched) specimens, at room temperature. Under torsion loads a number of nonlinear elastic effects were detected resulting in a control volume dependent on the loading mode. The volume radius under torsion resulted to be much greater than the radius under tensile loading. A non-conventional approach, based on the "apparent" linear elastic SED evaluated considering a different critical radius, allowed to overcome the problems tied to different extrinsic and intrinsic fracture mechanisms occurring under mode I and mode III loading. The term "apparent" seemed to be appropriate to describe the SED value measured without any clear distinction between non-linear intrinsic and extrinsic mechanisms and based on a linearelastic analysis of the stress distribution on the highly stressed zone ahead of the notch tip. A synthesis based on the apparent value of the linear elastic SED is only an engineering tool for strength assessments, the SED is applied to the room temperature data from torsion loads, despite the presence of large scale yielding.

The expression of R_c for mode III is reported here again for the sake of semplicity:

$$R_{3c} = \left(\sqrt{\frac{e_3}{1+\nu}} \cdot \frac{K_{3c}}{\tau_t} \right)^{\left(\frac{1}{1-\lambda_3}\right)} \tag{B.1}$$

The critical energy value can be obtained from the maximum shear strength τ_t by Beltrami's expression (3.3):

$$W_{3c} = \frac{\tau_t^2}{2G} \tag{B.2}$$

where G is the shear modulus. In Tab. B.1 are shown the values of K_{3c} and τ_t, from the experimental tests and of R_{3c} and W_{3c}, found by applying the values from Tab. 3.1 to Eqs. (3.1) and (3.3). The values are given for the room temperature case [35, 37, 38]:

Table B.1: Mode III experimental and critical values.

	Room Temperature
K_{3c} (MPa$\sqrt{\text{m}}$)	3.35
τ_t (MPa)	73.46
R_{3c} (mm)	0.61
W_{3c} (MJ/m^3)	3.37

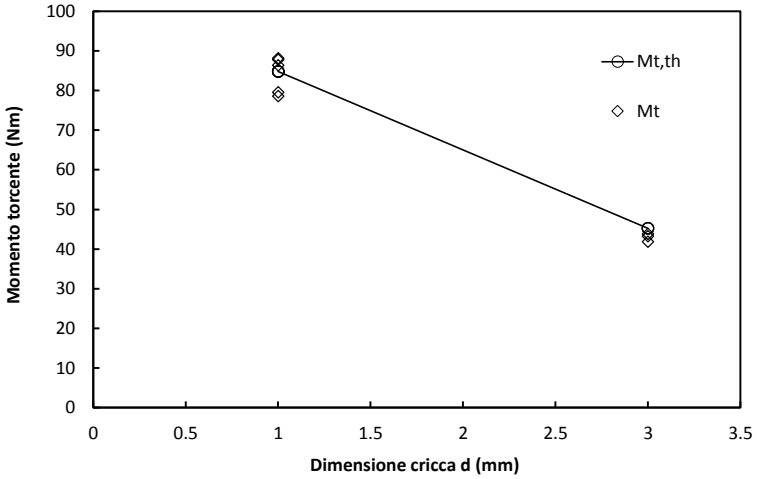

Figure B.1: Comparison between experimental data and theoretical assessment (M_{th} - open dot) for the PMMA cracked specimens, at room temperature.

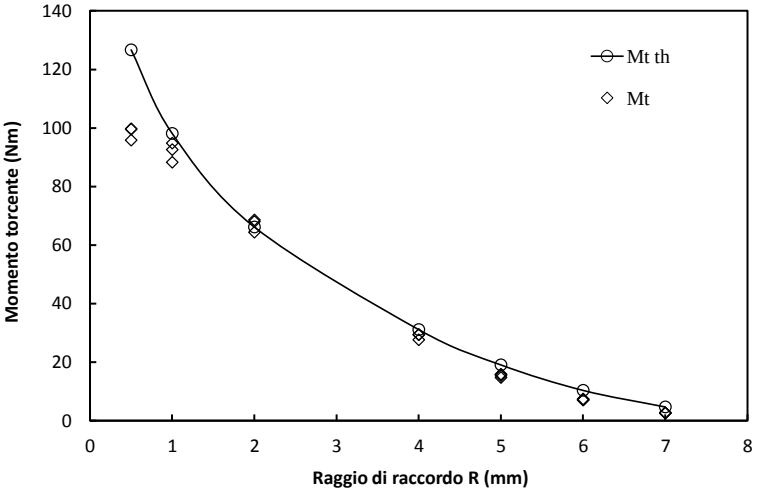

Figure B.2: Comparison between experimental data and theoretical assessment (M_{th} - open dot) for the PMMA semiciruclar notched specimens, at room temperature.

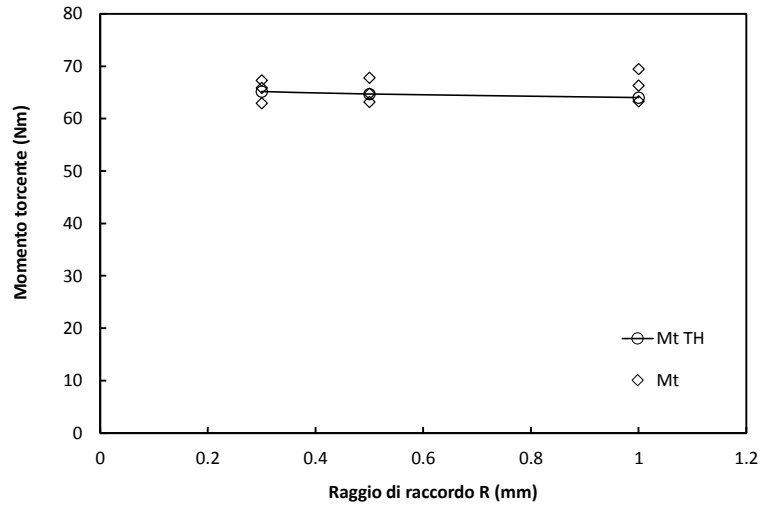

(a) U-noches

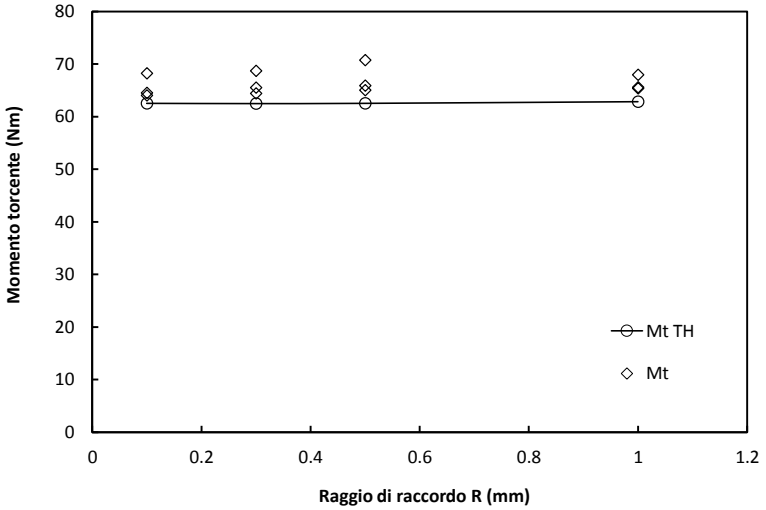

(b) V-noches

Figure B.3: Comparison between experimental data and theoretical assessment (M_{th} - open dot) for the PMMA specimens; a) U-shaped and b) V-shaped notches specimens, with d = 2 mm, at room temperature.

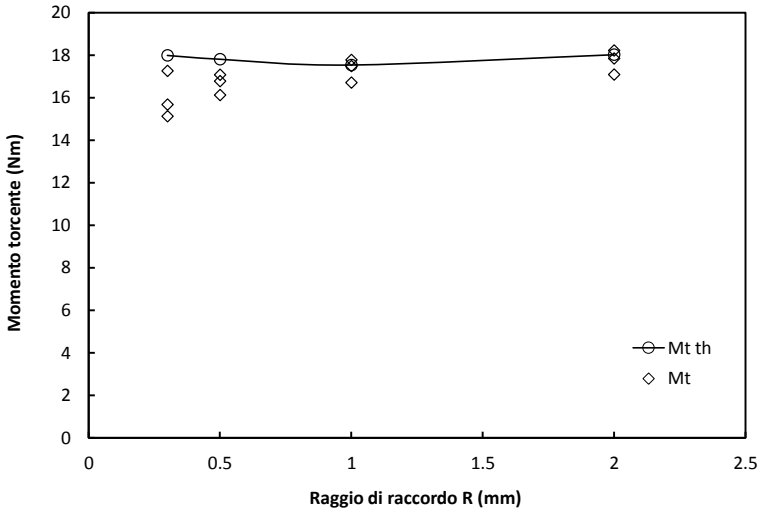

(a) U-noches

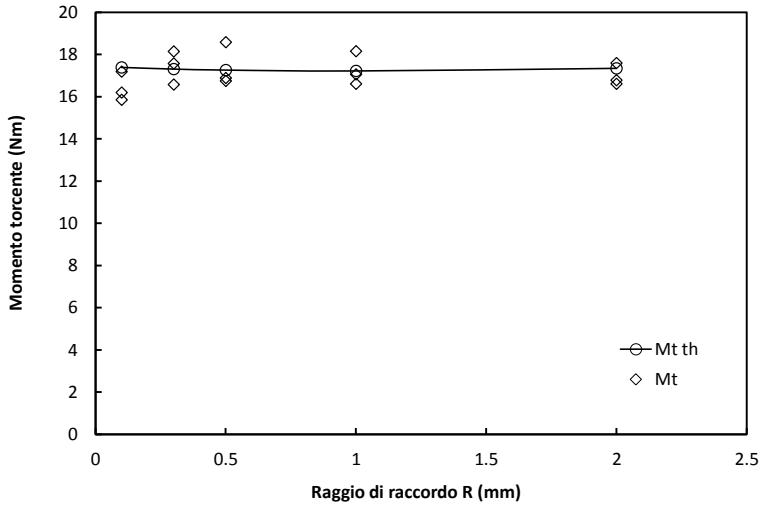

(b) V-noches

Figure B.4: Comparison between experimental data and theoretical assessment (M_{th} - open dot) for the PMMA specimens; a) U-shaped and b) V-shaped notches specimens, with d = 5 mm, at room temperature.

Appendix C

FEM models

In this section are reported some FE models examples, used to evaluate the NSIF and energy density over the control volume, in the torsion loading case.

In Figs. C.1, C.2 is shown the cracked specimen FE model, used to calculate the critical NSIF, K_{3c}. On every model was applied the displacement conditions shown in Fig. C.1, to ensure an axial-symmetric contions. In Fig. C.2 it is possible to note the spider web mesh made around the crack tip.

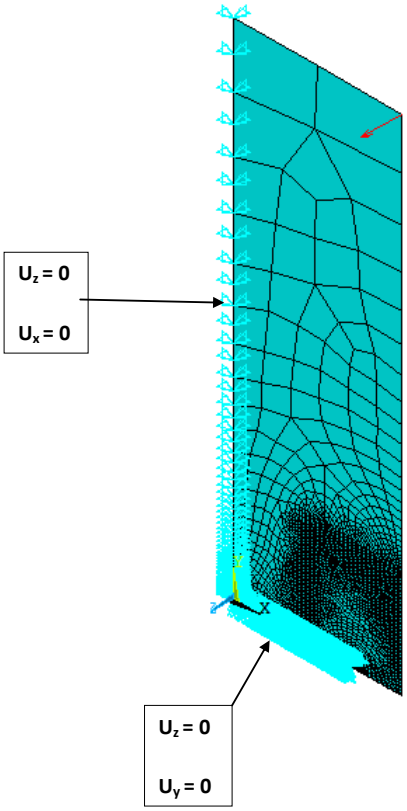

Figure C.1: Craked specimens model - displacement constraints.

FE models for U, V and semicircular notched specimens are reported in Figs. C.3-C.5, in wich are shown the used mesh and the control volume for each geometry.

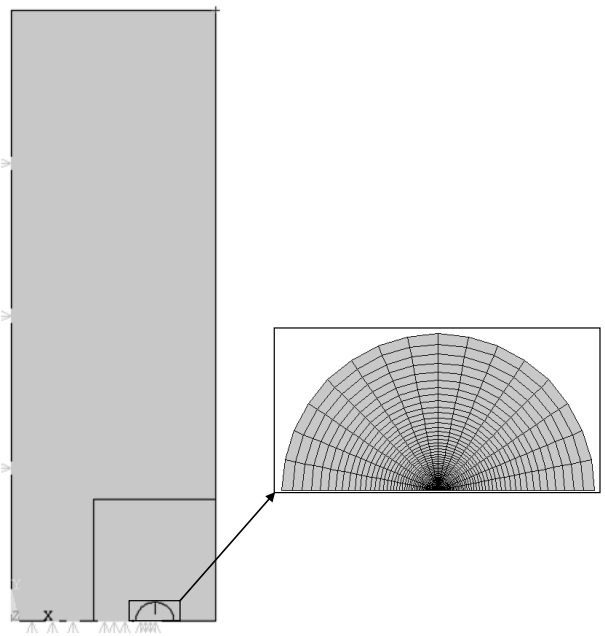

Figure C.2: Craked specimens model - spider web around the notch tip.

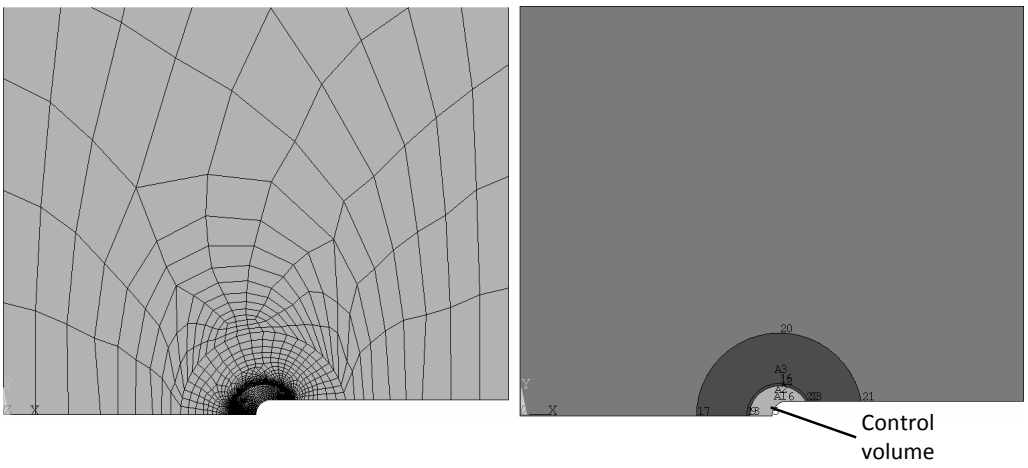

Figure C.3: U-notched specimens model - mesh and control volume.

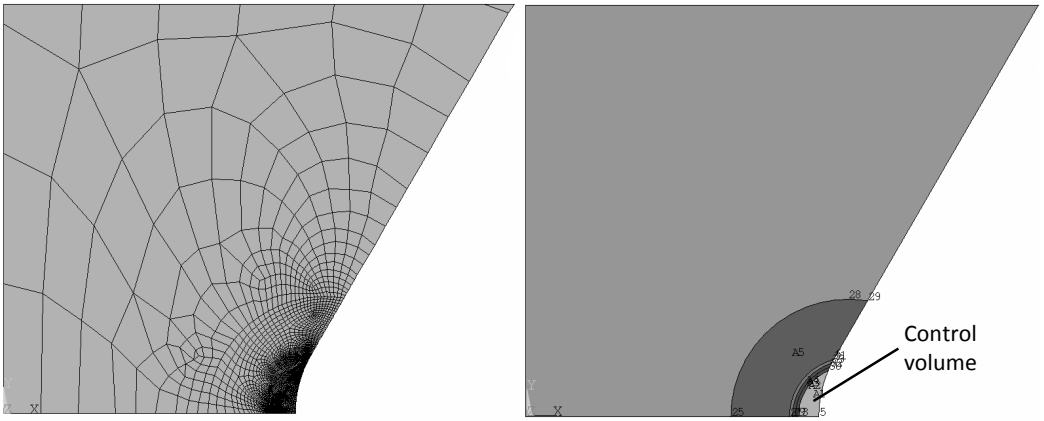

Figure C.4: V-notched specimens model - mesh and control volume.

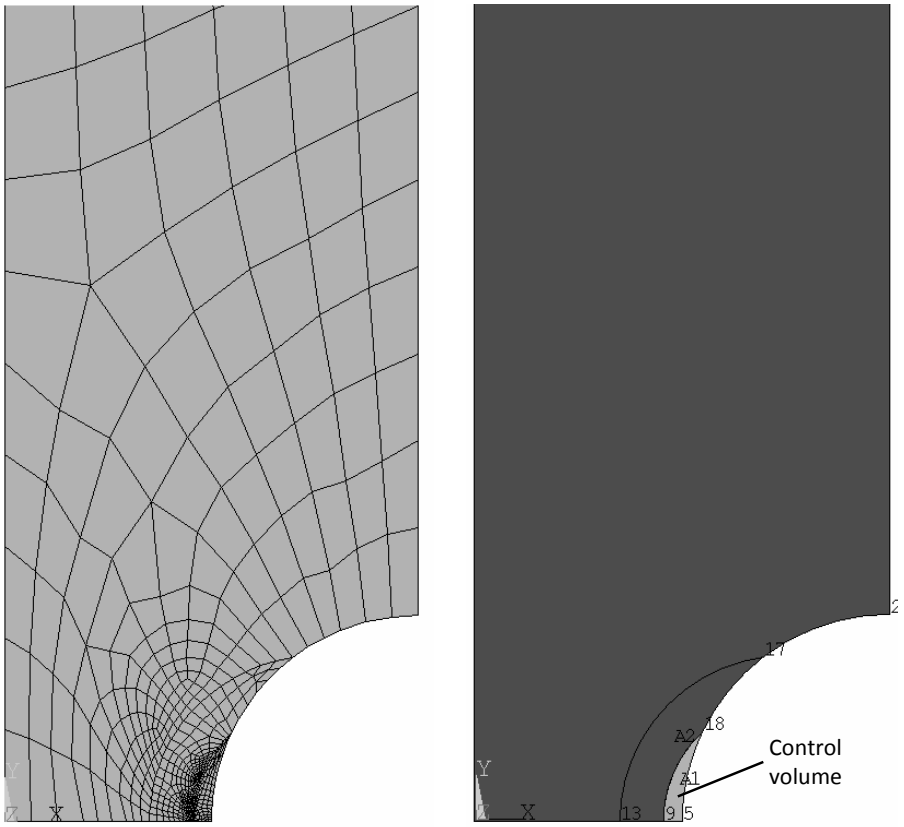

Figure C.5: Semicircular notched specimens model - mesh and control volume.